Regular Article
Geochemistry, Geophysics, Geosystems
DOI 10.1002/2013GC005012

Accepted Article

Modeling fluid flow in sedimentary basins with sill intrusions: Implications for hydrothermal venting and climate change

Karthik Iyer[1], Lars Rüpke[1] and Christophe Y. Galerne[2]*

[1]*The Future Ocean, GEOMAR, Wischhofstraße 1-3, D-24148 Kiel, Germany*

[2]*GeoModelling Solutions GmbH, Hardturmstraße 120, 8005 Zurich, Switzerland*

**Corresponding author: kiyer@geomar.de*

Abstract

Large volumes of magma emplaced within sedimentary basins have been linked to multiple climate change events due to release of greenhouse gases such as CH_4. Basin-scale estimates of thermogenic methane generation show that this process alone could generate enough greenhouse gases to trigger global incidents. However, the rates at which these gases are transported and released into the atmosphere are quantitatively unknown. We use a 2D, hybrid FEM/FVM model that solves for fully compressible fluid flow to quantify the thermogenic release and transport of methane and to evaluate flow patterns within these systems. Our results show that the methane generation potential in systems with fluid flow does not significantly differ from that estimated in diffusive systems. The values diverge when vigorous convection occurs with a maximum variation of about 50%. The fluid migration pattern around a cooling, impermeable sill alone generates hydrothermal plumes without the need for other processes such as boiling and/or explosive degassing. These fluid pathways are rooted at the edges of the outer sills consistent with seismic imaging. Methane venting at the surface occurs in three distinct stages and can last for hundreds of thousands of years. Our simulations suggest that although the quantity of methane potentially generated within the contact aureole can cause catastrophic climate change, the rate at which this methane is released into the atmosphere is too slow to trigger, by itself, some of the negative $\delta^{13}C$ excursions observed in the fossil record over short time scales (< 10,000 years).

Key points

- Fluid flow with methane transport in sedimentary basins with sill intrusion
- Hydrothermal complex forms as a direct result of flow pattern
- Flux of CH_4 alone cannot explain $-\delta^{13}C$ excursion over short time scales

This article has been accepted for publication and undergone full peer review but has not been through the copyediting, typesetting, pagination and proofreading process which may lead to differences between this version and the Version of Record. Please cite this article as doi: 10.1002/2013GC005012

© 2013 American Geophysical Union
Received: Aug 26, 2013; Revised: Oct 29, 2013; Accepted: Oct 31, 2013

Accepted Article

1. Introduction

Evidence of mass extinction events in conjunction with warming periods occur throughout the geological record. The processes that trigger such globally destructive change are still under considerable debate. Mass extinction events are defined as geologically short intervals (~ 1 My) during which life from multiple populations disappear on a global scale [*Ganino and Arndt*, 2009]. In recent years, volcanism has been closely linked with past climate variations and mass extinctions. Early studies proposed that the extinctions may have been caused due to poisoning from released trace metals [*Vogt*, 1972] or global cooling caused by volcanic ash and sulfate aerosols injected into the atmosphere [*Axelrod*, 1981] during huge volcanic eruptions. These climate events are also accompanied by pronounced negative carbon isotope excursions which are preserved in the fossil record and may be brought about by the release of vast quantities of light carbon into the atmosphere. A number of mechanisms have been proposed through which large quantities of light carbon may be released into the atmosphere resulting in climate variations and mass extinctions. For e.g., CO_2 released from lava degassing during the formation of Large Igneous Provinces (LIPs), which coincide with climate events over the past 300 Ma, have been linked to global warming [*Courtillot and Renne*, 2003]. However, the amount of CO_2 released during these eruptions from lava degassing is too small to trigger the carbon excursions connected to warming episodes. Additionally, the volume of lava erupted during these events does not correlate to the intensity of mass extinctions [*Wignall*, 2001]. *Dickens et al.* [1995] proposed that the negative $\delta^{13}C$ excursion accompanying the Paleocene-Eocene Thermal Maximum (PETM) approximately 55 My ago may be explained by a catastrophic release of isotopically light CH_4 by destabilizing sub-seafloor methane hydrate with a $\delta^{13}C$ value of -60‰. However, the uncertainty behind the process that destabilized hydrate, the relatively low global inventory of methane hydrate in the Paleocene and the discrepancy between the amount of warming and the carbon excursion pose significant challenges to this hypothesis [*Cohen et al.*, 2007; *Higgins and Schrag*, 2006]. Other mechanisms such as the burning and oxidation of a large proportion of terrestrial biomass [*Kurtz et al.*, 2003], overturn of stratified seawater under which isotopically light carbon had accumulated [*Küspert*, 1982] and the oxidation of light marine carbon after the uplift and desiccation of a shallow epicontinental seaway [*Higgins and Schrag*, 2006] are still questioned [*Cohen et al.*, 2007].

Thermogenic methane derived from contact metamorphism associated with magma emplacement and cooling in sedimentary basins has been recently gaining considerable

attention as a potential source of light carbon (e.g. [*Svensen and Jamtveit*, 2010]). LIPs such as the Siberian Traps, the Karoo-Ferrrar LIP and the North Atlantic Magmatic Province are associated with large volumes of volcanism and the formation of sill complexes within sedimentary basins [*Planke et al.*, 2005; *Svensen et al.*, 2012; *Svensen et al.*, 2004; *Svensen et al.*, 2009]. Here, organic-rich sedimentary rocks undergo thermal maturation within the contact aureole formed by the cooling of igneous intrusions. Greenhouse gases such as methane and carbon dioxide released by contact metamorphism can contribute to climate change when vented at the surface. The discovery of hydrothermal vent complexes that are spatially associated with such basins also supports the discharge of these gases into the atmosphere [*Jamtveit et al.*, 2004; *Planke et al.*, 2005; *Svensen et al.*, 2006]. Seismic studies show that vent initiation occurs mostly at sill tips [*Planke et al.*, 2005]. Hydrofracturing in sediments caused by overpressure due to boiling of pore fluid has been put forward as the driving force behind the formation of such vents [*Jamtveit et al.*, 2004]. The presence of brecciated sediments and rapidly quenched igneous material as well as hydrothermal minerals such as epidote and chlorite in these pipe structures also point to extensive fluid circulation [*Svensen et al.*, 2006; *Svensen et al.*, 2009].

Contact metamorphism of sedimentary rocks, therefore, has an enormous potential for climate forcing due to the large quantities of methane that could be liberated. However, the hydrothermal process accompanying this mechanism, which is key to understanding the transport and release of methane in this system, has not been suitably assessed. The goal of this study is to understand the flow pattern that may arise during sill emplacement in sedimentary basins and to quantify the out-flux of greenhouse gases generated at depth. We use a 2D, hybrid FEM/FVM model with an unstructured grid to evaluate fluid flow in a basin with a single saucer-shaped sill intrusion. The methane generated by organic cracking is constrained by calculating the vitrinite reflectance of the heated material and is transported with the pore fluid. The total amount of methane generated on a basin-scale is then extrapolated from the results and compared to previous estimates. Since the transport of methane is tracked, the flux of methane from the surface is also calculated, thereby providing insight into its possible effect on climate.

2. Mathematical model

Hydrothermal circulation has been often observed and reported as a significantly contributing effect to the process of contact metamorphism (e.g. [*Aarnes et al.*, 2010; *Galushkin*, 1997; *Planke et al.*, 2005; *Svensen and Jamtveit*, 2010; *Svensen et al.*, 2006]). However, previous

Accepted Article

models investigating the impact of contact metamorphism in sedimentary basins have either completely neglected or parameterized fluid flow in the contact aureole around sill intrusions. In order to better understand how fluid flow may influence the thermal maturation of host sediments during sill emplacement, we use a modified version of the FEM model developed and presented in *Iyer et al.* [2010] and *Iyer et al.* [2012].

2.1. Hydrothermal convection model

Hydrothermal convection is described by three governing equations. The first equation describes Darcy flow which relates the fluid velocity to the pressure gradient and buoyancy.

$$\vec{v}_f = -\frac{k}{\mu_f}\left(\nabla P - \rho_f \vec{g}\right) \tag{1}$$

The complete list of notations used in equations and their corresponding values is given in Table 1. Eq. (1) can be substituted in the mass conservation equation (2) yielding the fluid pressure equation (3).

$$\frac{\partial\left(\phi\rho_f\right)}{\partial t} = -\nabla\cdot\left(\rho_f \vec{v}_f\right) \tag{2}$$

$$\phi\frac{\partial\rho_f}{\partial t} = \nabla\cdot\left[\frac{k\rho_f}{\mu_f}\left(\nabla P - \rho_f\vec{g}\right)\right] - \rho_f\frac{\partial\phi}{\partial t} \tag{3}$$

The fluid density changes are split into its pressure and temperature equivalents giving

$$\phi\rho_f\beta_f\frac{\partial P}{\partial t} = \nabla\cdot\left[\frac{k\rho_f}{\mu_f}\left(\nabla P - \rho_f\vec{g}\right)\right] - \rho_f\frac{\partial\phi}{\partial t} + \phi\rho_f\alpha_f\frac{\partial T}{\partial t} \tag{4}$$

We use a fully compressible fluid formulation for the pressure equation with fluid properties of pure water corresponding to the IAPW-84 steam tables. It should be noted that the flow model is single phase and does not account for phase changes and boiling effects.

The energy equation accounts for diffusive and advective heat transfer and is written as

$$\left[\phi\rho_f c_{pf} + \left(1-\phi\right)\rho c_{peff}\right]\frac{\partial T}{\partial t} = -\rho_f c_{pf}\vec{v}_f\cdot\nabla T + \nabla\cdot\left(\kappa\nabla T\right) \tag{5}$$

Accepted Article

ρ is the rock or melt density, c_{peff} is the effective rock heat capacity and accounts for the latent heat of fusion in the crystallizing parts of the sill [*Aarnes et al.*, 2010; *Galushkin*, 1997],

$$c_{peff} = c_{pm}\left(1+\frac{L_C}{\left(T_L - T_S\right)c_{pm}}\right) \text{ for } \left[T_S < T < T_L\right]$$
$$c_{peff} = c_p \text{ for } \left[T_S > T\right] \tag{6}$$

2.2. Thermal maturation of organic matter in sediments and methane generation

The thermal maturity of a rock is the measure of the degree to which hydrocarbons are generated from organic material (kerogen) within sediments due to metamorphism. Although, the individual reactions are complex and mostly unknown, the entire process can be kinetically modeled by a number of twenty parallel first-order reactions described by an Arrhenius equation,

$$y\left(T\right) = A \times \exp\left(-\frac{E}{RT}\right) \tag{7}$$

where y is the temperature dependent reaction rate, A is the frequency factor, E is the activation energy, R is the gas constant and T is the absolute temperature (K). Vitrinite reflectance is a widely used indicator of thermal maturity and can be readily measure in the field. Here, we use the EASY%Ro method developed by *Sweeney and Burnham* [1990] to calculate the vitrinite reflectance and organic maturation based on the thermal history of the sediment. The method below has been described in detail by *Beardsmore and Cull* [2001].

For a given time period where the temperature within the source rock is increased from T_{t-1} to T_t from time *t-1* to *t*, the heating rate is

$$H_t = \frac{\left(T_t - T_{t-1}\right)}{\Delta t} \tag{8}$$

The parameter I_{it} is related to the rate of the i^{th} reaction over time period *t*,

$$I_{it} = T_t A\left[1-\frac{\left(E_i / RT_t\right)^2 + a_1\left(E_i / RT_t\right) + a_2}{\left(E_i / RT_t\right)^2 + b_1\left(E_i / RT_t\right) + b_2}\right]\exp\left(-E_i / RT_t\right) \tag{9}$$

Accepted Article

$$\Delta I_{it} = \Delta I_{it-1} + \frac{\left(I_{it} - I_{it-1}\right)}{H_j}$$
$$\Delta I_{i0} = 0 \tag{10}$$

The amount of unreacted material, W_{it}, remaining after the time interval t is

$$W_{it} = W_{i0} \exp\left(-\Delta I_{it}\right) \tag{11}$$

The total converted fraction, F, and the vitrinite reflectance, $\%Ro$, are calculated by

$$F = \sum_i f_i \left(1 - \frac{W_i}{W_{i0}}\right)$$
$$\%Ro = \exp\left(-1.6 + 3.7F\right) \tag{12}$$

E_i and f_i in Eqns. (9) and (12) are the activation energy and weighting factors, respectively, for the i^{th} reaction. The values can be found in *Sweeney and Burnham* [1990].

The rate of organic matter degradation by thermal cracking can be calculated by

$$R_{om} = -\left(1-\phi\right)\rho_{hr}\frac{\partial TOC}{\partial t}$$
$$TOC = TOC_0 F\left(t\right) \tag{13}$$

Similar to *Aarnes et al.* [2010], we assume that all the hydrocarbons are converted into methane within the gas window where the vitrinite reflectance (%Ro) is greater than 1% and the rate is calculated by,

$$R_{CH_4} = R_{om} m_{CH_4} \tag{14}$$

2.3. Dehydration reactions

Mineral dehydration reactions release fluids into the system and occur as the sediment heats up and causes mineral phase changes. The phase changes will depend on the original mineralogy of the sediment and is modeled using the composition of an average pelite [*Caddick and Thompson*, 2008] and based on equilibrium thermodynamics [*Connolly and Petrini*, 2002]. The water content for the rock composition is pre-calculated over a range of temperatures and pressures and depends on the stable mineral assemblage. The rate of water generated by dehydration reactions is,

$$R_D = -\left(1-\phi\right)\rho_{hr}\frac{\partial Wa}{\partial t} \tag{15}$$

Accepted Article

Sections 2.2 and 2.3 are based on previous work by *Aarnes et al.* [2010] where more details can be found.

Dehydration reactions and organic maturation within the sediments affects the energy distribution and the mass conservation equation. In order to account for the latent heat of dehydration and organic maturation, the energy equation (5) is modified to

$$\left[\phi\rho_f c_{pf} + (1-\phi)\rho c_{peff}\right]\frac{\partial T}{\partial t} = -\rho_f c_{pf}\vec{v}_f \cdot \nabla T + \nabla\cdot(\kappa\nabla T) - L_D R_D - L_{OM} R_{OM} \quad (16)$$

The mass conservation equation (2) is modified to account for the generation of fluids during sediment dehydration with a source term by,

$$\frac{\partial(\phi\rho_f)}{\partial t} = -\nabla\cdot(\rho_f\vec{v}_f) + R_D \quad (17)$$

The pressure equation is consequently modified to

$$\phi\rho_f\beta_f\frac{\partial P}{\partial t} = \nabla\cdot\left[\frac{k\rho_f}{\mu_f}(\nabla P - \rho_f\vec{g})\right] - \rho_f\frac{\partial\phi}{\partial t} + \phi\rho_f\alpha_f\frac{\partial T}{\partial t} + R_D \quad (18)$$

3. Model setup

The model reproduces a single large sill emplaced in a sedimentary basin in LIPs that can be part of a much larger sill complex such as the Karoo Basin, South Africa [*Chevallier and Woodford*, 1999; *Galerne et al.*, 2008] and in the Vøring and Møre basins offshore Norway [*Planke et al.*, 2005]. Many of these large sills exhibit a saucer-shape and comprise of three distinct segments: (1) a sub-horizontal inner sill that forms the base transitioning to, (2) a steep inclined sheet cross-cutting sedimentary strata which ends in (3) a sub-horizontal outer sill [*Chevallier and Woodford*, 1999; *Galerne et al.*, 2011; *Polteau et al.*, 2008]. The emplacement mechanism of saucer-shaped sills may be controlled by the level of neutral buoyancy of the magma or horizontal discontinuities present in the sediments and has been extensively described in the literature [*Barker*, 2000; *Malthe-Sorenssen et al.*, 2004]. The modeled domain is a 10 km wide and 2 km deep box containing a uniform lithology composed of pelitic sediments with 5 wt% TOC content and representing a sedimentary basin (Fig. 1). The temperature within the box is initialized to a shallow geotherm with an increase in temperature of 30°C per km and a surface temperature of 2°C. The bottom boundary

Accepted Article

temperature is kept fixed at the initial temperature for the duration of the simulation. Fluid can enter and exit the domain freely through the top boundary and no flow conditions are applied to the sides and the bottom. The top surface is kept a fixed pressure of 22 MPa corresponding to a water depth of 2.2 km to suppress phase changes in a single phase model. This pressure boundary condition is valid for submarine environments such as the Vøring and Møre basins but is problematic in subaerial systems. On the other hand, fluid boiling at sub-critical pressures may result in explosive venting which is also observed in the field as breccia pipes at shallow levels (e.g. [*Svensen et al.*, 2006]). The surface of our domain is, therefore, a proxy for the depth above which fluid venting into the atmosphere or ocean takes place over very short time scales and is assumed to be instantaneous. A 100m thick saucer-shaped sill is instantaneously emplaced at a depth of 1.1 km and a temperature of 1150°C approximating that of a mafic melt. The inner sill is 5 km long transitioning to the inclined sheets that dip upwards at an angle of 30° to 200 m above the inner sill and then leveling out to form 200 m long horizontal outer sills on either side [*Chevallier and Woodford*, 1999; *Galland et al.*, 2009; *Polteau et al.*, 2008]. The initial porosity of the sediments is depth-dependent and is given by,

$$\phi = \phi_s \exp(-zm) \tag{19}$$

where φ_s is the surface porosity, z is the absolute depth below the seafloor (m) and m is a constant. The permeability is related to the porosity and is described by a simplified Kozeny-Carman equation (e.g. [*Costa*, 2006])

$$k = k_0 \left[\frac{\phi^{n+1}}{(1-\phi)^n} \right] \tag{20}$$

where k_0 and n are constants.

4. Results

We conducted a set of numerical experiments in order to better understand the role of fluids during sill intrusion within sedimentary basins and its impact on thermal maturation of organic matter. The thickness of the thermal aureole and the gas zone are defined as the region where %Ro≥1 in all simulations.

Accepted Article

4.1. Reference Case (Thermal diffusion only)

The reference case involves only thermal diffusion in which the 100m thick saucer-shaped sill cools down to approximately 200°C in just 1500 years and to ~125°C in 5000 years (simulation end). Heating of the surrounding sediments results in a contact aureole approximately 120m thick above and below the flat parts of the intrusion (Fig. 2). Dehydration reactions and thermal cracking also occur as the sediments are heated and go to completion within 1000 years after sill emplacement. The amount of water released during these reactions in the gas zone ranges from a maximum of 105 kg/m^3 to a minimum of 15 kg/m^3. The minimum and maximum amount of methane released in the gas zone due to thermal maturation for sediments with TOC content of 5% are 70 kg/m^3 and 137 kg/m^3, respectively. The total amount of methane released within the simulated domain is 130,000 tons. In order to compare the amount of methane generated to other studies [*Aarnes et al.*, 2010], we take the amount of methane generated in a single column above and below the sill averaged over the entire domain and then sum the column to obtain units of kg/m^2. This amount is then multiplied by the area covered by sills to obtain the methane generation potential in sedimentary basins. The total area covered by sill intrusions in the Vøring and Møre basins in the North Atlantic Volcanic Province has been estimated at 85,000 km^2 [*Svensen et al.*, 2004] while the area covered in the western Karoo Basin is 50,000 km^2 [*Svensen et al.*, 2007]. Using the results from the reference case, the total amount of methane that may be generated in these areas are 2200 and 1300 Gt, respectively and is comparable to the amounts estimated by *Aarnes et al.* [2010].

4.2. Thermal effects of sill intrusion with fluid flow

The model parameters in this simulation are identical to those in the reference case with the addition of fluid flow. Here, the energy equation is modified to account for advective heat transfer by the fluid (Eq. (16)). Additionally, release of water during mineral dehydration results in an increase in fluid pressure (Eq. (18)). The surface porosity and permeability constant used in Eq. (19) and (20) is 0.3 and 10^{-13} m^2, respectively. Porosity in the domain decreases by an order of magnitude with depth and permeability decreases by more than two orders of magnitude from $8x10^{-15}$ m^2 at the surface to $3x10^{-17}$ m^2 at the bottom. The simulation is run for 5000 years at which point the maximum temperature within the sill is 130°C. Although, vigorous fluid convection is not observed due to the relatively low rock permeability, fluid flow does occur and somewhat influences the thermal evolution of the

Accepted Article

sediments surrounding the cooling intrusive (Fig. 3). Fluid flow initiates soon after sill emplacement. Hot fluids around the inner sill rise along the top and bottom edges of the inclined sheet. This results in a slowly rising plume of hot fluid at the outer sills on both sides of the intrusive. These fluids eventually vent at the surface at relatively low temperatures (<45°C) after ~1500 years. The contact aureole is 120m thick around the inner sill and is similar to that obtained in the reference case after 5000 years. The contact aureole reaches a thickness of up to 200m in the plume region above the outer sills and consequently results in enhanced thermal maturation and methane generation in this part of the domain (Fig. 4). The maximum and minimum amount of water released during sediment dehydration in the gas zone is 120 kg/m^3 and 15 kg/m^3 respectively. The maximum and minimum amount of methane generated due to thermal cracking of organic material in the gas zone is 137 kg/m^3 and 70 kg/m^3 respectively. The total amount of methane generated in the domain is slightly greater than the reference case at 155,000 tons. Using the results from this simulation, the total methane potential of the Vøring and Møre basins and the western Karoo basin is 2500 and 1500 Gt, respectively.

4.2.1. Effect of permeability and porosity

The key factor that controls the intensity and pattern of fluid flow is the rock permeability and to some extent the porosity. Permeability is a property that is dependent on the rock type, its formation and deformation history. Sedimentary rocks have an extremely wide range of permeability that can vary from 10^{-11} m^2 for carbonates and sandstones to 10^{-19} m^2 for mudstones and shale (e.g. [*Doyen*, 1988; *Ehrenberg et al.*, 2006; *Reece et al.*, 2012; *Revil and Cathles*, 1999]). We conducted additional simulations using the setup described in section 3 and changed the permeability constant in Eq. (20) to investigate the effect of permeability on fluid flow and subsequently the thermal structure and methane generation in basins with varying sediment infill. The permeability constant, k_0, is varied from 10^{-15} m^2 resulting in a surface and bottom permeability of $8\text{x}10^{-17}$ m^2 and $3\text{x}10^{-19}$ m^2, respectively, to 10^{-12} m^2 resulting in a surface and bottom permeability of $8\text{x}10^{-14}$ m^2 and $3\text{x}10^{-16}$ m^2, respectively. Fluid flow does not considerably affect the thermal structure in simulations where the permeability structure is low ($k_0 \leq 10^{-14}$ m^2). The contact aureole and methane potential calculated from these simulations are the same as those derived in the reference case where only thermal diffusion occurs. On the other hand, fluid flow dominates simulations with increased permeability and results in vigorous convection. Early plumes form at the ends of the outer sills due to the confluence of fluids from the upper and lower parts of the sill similar to the simulation mentioned in Section 4.2 and vent at the surface at temperatures of about

Accepted Article

220 and 270°C initially when the permeability constant is $5x10^{-13}$ m^2 and 10^{-12} m^2, respectively (Fig. 5a and b). The increased vent temperatures are a direct result of high permeabilities and therefore the system is still rather hot when venting occurs. Due to increased permeability, multiple convection cells form at the top of the inner sill after a sufficiently thick thermal boundary layer is formed. The cells merge with each other as they grow and eventually some of them vent at the surface but much after the outer sill plumes make their way to the surface and also at lower temperatures (~60-150°C) (Fig. 5c and d). Vitrinite reflectance and the generation of methane are controlled by the thermal history of the sediments which in turn depends on the flow regime. A column of mature organic material with high vitrinite reflectance is generated above the outer sills where the initial plumes form. The contact aureole below the sill is similar to that obtained in the reference case. However, the contact aureole follows the multiple convective cells above the inner sill that are generated by rising hot fluids resulting in an uneven distribution of thermal maturation in sediments. The amount of methane generated within the simulated domain in these cases where fluid flow rather than diffusion controls the final thermal structure can be up to 200,000 tons. This translates to a methane generation potential of 3350 Gt and 2000 Gt for the Vøring and Møre basins and the western Karoo basin, respectively.

4.3. Methane transport

Previous studies calculated the prospective methane based on maturation of sediments around the intrusion due to thermal diffusion only. The methane produced in these systems is assumed to immediately leave the system and vent into the atmosphere. Although, this is an important first step to determine methane potential on a basin-scale, the amount and rate at which methane may escape out of the geological system, which has important repercussions with regard to climate change, is still not quantified. Therefore, in order to better constrain these unknowns, we track the fluid pathways in the simulated domain and calculate the flow of methane out of the system from the surface. The single-phase flow model uses some simplifications to do this: (1) the methane produced moves with the fluid velocity and (2) methane and fluid within the pore space exist as a single, mixed phase. The methane generated in the sediments is advected using the Finite Volume Method which is mass conserving. The finite volumes employ a second-order accurate, TVD scheme and are based on the existing finite element mesh such that each volume is centered on a finite element node. Details on the implementation of a hybrid finite element - finite volume method is given

Accepted Article

in *Geiger et al.* [2004]. The differential form of the mass conservation equation used to track methane advection with finite volumes is given by:

$$\frac{\partial M_{CH_4}}{\partial t} = -\nabla \cdot \left(M_{CH_4} \vec{v}_f \right) + R_{CH_4} \tag{21}$$

where the M_{CH4} is the mass of methane per unit volume and R_{CH4} is the amount of methane generated due to thermal maturation of sediments obtained from Eq. (14).

The density of pure methane at temperatures and pressures experienced by the fluid in the modeled domain is similar to approximately 10% of the density of pure water. For e.g., the densities of methane and pure water at 250°C and 30 MPa are 102 and 826 kg/m^3, respectively [*Setzmann and Wagner*, 1991]. The density of methane-bearing fluid is, therefore, linearly varied such that fluid containing 120 kg/m^3 CH_4 or more has a density equivalent to 10% of pure water at the same temperature and pressure. Additional experiments using a linear density function for methane-bearing fluids with a minimum density equivalent to 1% and 50% of the density of pure water do not show significant changes in the cumulative rates at which methane is released from the domain surface (Fig. 6). The surface porosity and permeability constant values used in these experiments are 0.3 and between 10^{-14} and $5\text{x}10^{-13}$ m^2, respectively and the model setup is identical to the one in Section 4.2. The simulations are run for a much longer time period (100,000 to 400,000 years) as methane venting at the surface still occurs much after the system has completely cooled. Similar to the experiment presented in Section 4.2, heating of fluids results in flow towards the outer sill and generates a plume of hot fluids at top of the outer sill at both ends of the intrusion where fluids from above and below the sill merge together. Methane generated during thermal cracking of organic matter is advected with the fluid and accumulates at the top of the outer sills where fluids merge. The high buoyancy of the fluids, a product of increased temperatures and methane content, in these regions results in a relatively rapid rise of fluid towards the surface (Fig. 7). Vent temperatures reach a maximum of approximately 95°C which is twice greater than those in the simulation where methane is not transported ($k_0 = 10^{-13}$ m^2). This occurs as the low-density, methane-rich fluids require relatively less time to reach the surface and occurs as early as ~200 years when the system is hotter. The build-up of methane above the inner sill results in low density fluids that migrate upwards in finger-like plumes which ultimately reach the surface. This results in a slightly uneven thermal structure above the intrusion but is not much different from that in Section 4.2. Venting of this methane-rich fluid initiates after just ~640 years and continues till 100,000 years after which

Accepted Article

most but not all of the methane above the sill has been transported and released into the atmosphere (Fig. 8). The total amount of methane generated within the domain due to organic cracking is between 140,000 and 180,000 tons and is similar to the experiments in Section 4.2.

A simulation in which the permeability of the sill was linearly increased from the initial value to the depth-dependent background value for temperatures between 700°C and 500°C, respectively, investigated the effect of inward fracture propagation during cooling and crystallization of the sill. The permeability constant for this simulation is $5x10^{-13}$ m^2 while the other parameters are kept the same. Sill permeability increases after only ~140 yrs when the system has cooled below 700°C. Buoyant, methane rich plumes generated at the outer sill reaches the surface after ~165 years. Due to the increasing permeability of the cooling sill, methane generated beneath the sill can now migrate upwards through the sill itself. Due to the relatively increased fluid activity generated by the permeable sill, the total amount of methane generated in this case is 205,000 tons which is higher than the simulation with an impermeable sill (180,000 tons).

A final set of simulations explored the effect of sill emplacement depth on the amount of methane generated in the thermal aureole and the rate of degassing of methane at the domain surface. The sill emplacement depth is increased in 500m intervals as compared to the original setup in section 3 up to a maximum depth increase of 1500m. The domain depth is also increased accordingly and the bottom temperature boundary condition is changed such that the thermal gradient used in the original setup remains unchanged. The permeability constant used in this set of simulations is 10^{-13} m^2. The total amount of methane generated within the domain increases with increasing depth of emplacement (from 155,000 to 210,000 tons) due to the relatively higher temperatures at depth which results in a larger contact aureole. Fluid flow and methane accumulation at the outer sill similar to the previous simulations also occurs irrespective of the sill depth. However, the time taken for the hydrothermal plume to reach the surface increases with increasing sill depth due to lower permeabilities that are encountered deeper within the domain and also due to the fact that the distance from the outer sill to the domain surface increases.

Accepted Article

Accepted Article

5. Discussion

5.1. Sill intrusions and hydrothermal venting

Hydrothermal and phreatomagmatic vent complexes have been found in sedimentary basins linked to LIPs all over the world which include the Vøring and Møre basins [*Planke et al.*, 2005; *Svensen et al.*, 2003], the Karoo Basin in southern Africa [*Jamtveit et al.*, 2004; *Svensen et al.*, 2006] and the Tunguska Basin in Russia [*Svensen et al.*, 2009] to name a few. 2D and 3D seismic imaging in the Vøring and Møre basins have additionally revealed a spatial relation between sill intrusions at depth and hydrothermal vents [*Planke et al.*, 2005]. Hydrothermal vents act a conduits for fluid and gas phases originating within the contact aureole of the associated sill intrusion and form eyes, craters or mounds at the paleosurface [*Planke et al.*, 2005]. One of the hypothesis by which the hydrothermal vent forms at depth is due overpressure in the sediments [*Aarnes et al.*, 2010; *Jamtveit et al.*, 2004; *Planke et al.*, 2005; *Svensen et al.*, 2006]. Boiling of pore fluids and fluids released during metamorphic dehydration reactions due to sediment heating in the contact aureole will result in a large volume increase. This volume increase then results in fluid overpressure and may initiate hydrofracturing within the sediment. Rock hydrofracturing causes the upward migration of these hot, buoyant fluids and results in the formation of a pipe conduit. However, boiling of fluids in the contact aureole only occurs to a depth of less than 1 km below which the fluid is supercritical and, therefore, cannot explain deep-rooted hydrothermal vent complexes that have been seismically imaged in the Vøring and Møre basins (Fig. 4 in *Planke et al.* [2005]). On the other hand, it can be argued that hydrofracturing at greater depths is instead caused by the release of large volumes of low-density gas phases such as CO_2, CH_4 and SO_2 during thermal maturation of the heated sediments [*Aarnes et al.*, 2010]. The process of hydrofracturing may well be valid in low permeability rocks where fluids cannot readily escape leading to a build-up in pressure but the process cannot occur in rocks with relatively higher permeabilities where fluid seepage would effectively reduce any excess pressure required for the initiation of hydrofracturing [*Jamtveit et al.*, 2004]. Moreover, the majority of hydrothermal vent complexes originate at the tips of sill intrusions at varying depths [*Planke et al.*, 2005]. If boiling and/or excessive gas generation is the main process resulting in vent formation, one would expect the vent source to occur within any region of the contact aureole above the sill where boiling would be expected to take place. Our results, on the other hand, show that fluid flow alone, irrespective of the convective vigor, can be the controlling process behind the generation of hydrothermal vents and their spatial relation with sill intrusions. The emplacement of hot magma within a sedimentary basin heats up the surrounding fluids and

results in thermal cracking of the sediments. Hot, buoyant and methane-rich fluids below the sill cannot migrate directly upwards due to the presence of an impermeable sill and, therefore, move outwards along the edges and around the sides of the sill (Fig. 3). Once the fluids flow around the sill, they migrate upwards to vent at the surface. In the case of saucer-shaped sills, the formation of hydrothermal plumes at the outer-sill is enhanced by fluids above the sill migrating upslope along the inclined sheets resulting in more focused fluid flow. The same experiment performed with a flat sill also shows methane-rich hydrothermal plumes initially forming at the sill sides and venting at the surface. Sedimentary breccias may be formed due to explosive venting caused by rapid decompression of the ascending fluids and gases but are observed only at shallow levels of such hydrothermal complexes [*Planke et al.*, 2005; *Svensen et al.*, 2006]. Therefore, although hydrofracturing due to boiling and/or gas release processes are not explicitly required to initiate vent formation rooted at sill edges, they may play a more significant role in shallow systems where phase changes may occur. Fluid flow around a cooling sill is by itself enough to form hydrothermal vents at the outer sill consistent with seismic observations.

5.2. Methane release and climate effects

Previous studies have shown that global climate variations may be linked to degassing of greenhouse gases such as CO_2 and CH_4 during metamorphic reactions over very large scales. *Courtillot and Renne* [2003] and *Wignall* [2001] presented reviews showing that global warming, mass extinction and marine anoxia events are temporally connected to the formation of LIPs at least over the past 300 Ma. Over this period, correlations have been found between the end-Guadalupian event and the Emeshian volcanic province [*Ganino and Arndt*, 2009; *Zhou et al.*, 2002], the end-Permian event and the Siberian traps [*Retallack and Jahren*, 2008; *Svensen et al.*, 2009], the end-Triassic event and the Central Atlantic Magmatic province [*Courtillot and Renne*, 2003], the early Toarcian event and the Karoo-Ferrar Traps [*Svensen et al.*, 2007], the end-Cretaceous event and the Deccan Traps [*Courtillot and Renne*, 2003] and the PETM and the North Atlantic igneous province [*Svensen et al.*, 2004]. Although, degassing of magmatic volatiles such as CO_2 alone during such LIP events is not enough to trigger such catastrophic incidents, the amount of sediment-derived carbon is 11-26 times greater than the magmatic reservoir [*Ganino and Arndt*, 2009]. This led to the hypothesis that the generation of methane in the contact aureoles around igneous sills may be the driving force behind climate change. However, although the amount of thermogenic

Accepted Article

Accepted Article

methane has been quantified on a basin scale, the rate at which this may flux into the atmosphere, which is crucial to evaluating its effect on climate, remains unknown.

Here, we investigate the process by which methane is transported towards the surface during thermogenic maturation of sediments. Previous studies that have estimated the release of thermogenic methane assume that all of the generated methane is instantaneously and completely released into the atmosphere (e.g. [*Aarnes et al.*, 2010; *Svensen et al.*, 2007]). Modeling the transport of methane shows that venting of this greenhouse gas into the atmosphere/ocean after generation at depth depends on the mobility of the phase which in turn depends on rock properties such as permeability. Time scales over which significant venting takes place can range from a few thousand years for permeable systems to a hundreds of thousands of years in systems with lower permeabilities. As described in sections 4.2 and 4.3, an initial outburst of methane at the surface occurs as the primary plumes generated at the outer sills reaches the surface (Fig. 8). This initial discharge gradually tapers off and is later rejuvenated, albeit at much lower levels, as methane-rich fluids present above the inner sill make their way to the surface and the system cools down. The timing of the initial and later methane fluxes will depend on the permeability of the system. The initial methane burst occurs just 207 years after sill emplacement in systems with higher permeabilities (k_0=5x10^{-13} m^2) but can take up to 6300 years when permeability is lower (k_0=10^{-14} m^2). More importantly, methane generated below the sill takes a very long time to reach the surface if the sill remains impermeable. The buoyant, methane-rich fluid beneath the sill tends to migrate directly upwards thus trapping it below the sill. Very slow lateral movement of this fluid towards the outer sills results in a gradual seepage of methane at the surface over hundreds of thousands of years. Although, some percentage of methane is left behind in most simulations, simulations with sills that are sub-horizontal show that the tilt of the intrusion facilitates the migration of fluids below the sill towards the surface, mostly at the shallower outer sill. Complete methane degassing can only occur if the sill is permeable as shown in the simulation where the permeability of the sill is increased to the background value due to fracture formation and propagation as the sill cools. In essence, methane release at the surface of the sedimentary basin occurs over three stages (Fig. 9):

1. The first stage of methane release occurs as the hydrothermal plumes formed at the outer sills reach the surface. This results in sharp peak in outward methane fluxes over a short time period and accounts for up to ~30% of the total methane generated in the basin.

2. The second stage of methane release at the surface takes place over a longer time period (≥ 400,000 years in systems with low permeability (Fig. 9a)) during which methane generated above the inner sill makes it way to the surface in finger-like plumes at velocities lower than the initial hydrothermal plumes. Up to 75% of the total methane produced in the basin is released out of the domain by the end of this stage.
3. The third stage consists of the slow degassing of methane from the below the sill and occurs for many hundreds of thousands of years. Some methane may still be left behind in the basin.

Also, the amount of methane generated increases with increasing sill emplacement depth due to larger contact aureoles resulting from higher temperatures deeper below the surface. Although, three-stage methane degassing is also observed with increasing sill depth, fluid flow around the sills is slower due to lower permeabilities deeper within the domain. Subsequently, it takes longer for the initial plumes to reach the surface and also for methane degassing to take place (Figs. 10a-c). The total amount of methane generated within the contact aureole and the rate of methane degassing at the surface is linearly related to the emplacement depth (Fig. 10d). A summary of methane fluxes at the surface for different numerical experiments and the time scales over which it occurs is outlined in Table 3.

The climate and LIP events also coincide with negative carbon isotope incursions in the fossil record and may be explained by the release of $\delta^{13}C$-depleted gases (e.g. [*Cohen et al.*, 2007; *Dickens et al.*, 1997; *Dickens et al.*, 1995; *Higgins and Schrag*, 2006; *Pagani et al.*, 2006; *Retallack and Jahren*, 2008]). The PETM is characterized by a $\delta^{13}C$ incursion of -2 to -3‰ over 10,000 years and is temporally associated with the formation of the North Atlantic igneous province. *Svensen et al.* [2004] estimated that between 300 and 3000 Gt of methane could have been released due to thermal cracking of organic matter in the Vøring and Møre basins resulting in a carbon isotope excursion of -0.2 to -3.0‰ using values of present-day exchangeable carbon reservoir and a $\delta^{13}C$ value of -60‰ for the released methane. Thermogenic methane produced by cracking of organic matter in sediments within the contact aureole has a depleted carbon isotope ratio ($\delta^{13}C$ = -35 to -50‰) [*Svensen et al.*, 2004]. However, the average $\delta^{13}C$ value tends towards an average of -35‰ if large amounts of thermogenic methane is generated [*Higgins and Schrag*, 2006]. Using a thermal diffusion model and a sediment TOC content of 6 wt%, *Aarnes et al.* [2010] showed that 3500 Gt of CH_4 released in the Vøring and Møre basins can result in a -2.5‰ shift in $\delta^{13}C$ values using a

Accepted Article

carbon isotopic composition of methane of -35‰. However, the time scale over which methane released by thermogenic processes is discharged into the atmosphere is unclear.

We use the method proposed by *Dickens et al.* [1995] to estimate the magnitude of the carbon isotope ratio excursion based on the surface methane fluxes obtained from our model. Simulations of methane transport towards the basin surface reveal that only part of the total methane generated reaches the surface over a period of 10,000 years. Sedimentary basins with very low effective permeabilities vent only up to 5% of the total CH_4 at the surface within the first 10,000 years (Fig. 9a). This number increases appreciably as permeability increases; between 45 and 80% when the permeability structure increases by only a couple of orders of magnitude (Figs. 9b and c). The presence of tilted sills also results in an increased flux of methane at the surface over similar time scales (Fig. 9d). The methane generation potential within the Vøring and Møre basins ranges from 2200 to 3350 Gt when the sediment TOC content is 5 wt% (see section 4). Therefore, the total flux of methane from these basins into the atmosphere over 10,000 years ranges between 1200 and 2200 Gt (45 and 80%) using an average CH_4 generation potential of 2750 Gt. This would result in a $\delta^{13}C$ excursion of only -0.7 to -1.2‰ if the $\delta^{13}C$ value of methane is -35‰, which is not enough to explain that observed in the fossil record. The average methane generation potential increases to 3100 Gt if a TOC content of 6 wt% is assumed. The resulting $\delta^{13}C$ excursion is -0.8 to -1.4‰ if 45 and 80% of the total methane generated escapes into the atmosphere, respectively. Even if a TOC content of 10 wt% is assumed, the average methane generation potential is 5000 Gt and in turn results in a maximum $\delta^{13}C$ excursion of -2.1‰.

The formation of a LIP in the Karoo Basin also coincides with a major carbon isotope excursion between -3 and -6‰ in the Toarcian [*Cohen et al.*, 2007; *Svensen et al.*, 2007]. The methane generation potential for this basin averaged over the various simulations and a sediment TOC content of 5 wt% is 12,600 Gt. The magnitude of the initial shifts in the carbon record for the Toarcian event are between -1.5 and -3‰ and occurred in less than 2000 years [*Cohen et al.*, 2007]. The simulated atmospheric methane flux for the first 2000 years is between 20 and 60% of the total methane potential and results in a $\delta^{13}C$ shift of -1.3 and -3.8‰, respectively. Although the higher shift value can effectively explain the excursion accompanying the Toarcian event, the values calculated here assume that the entire basin area is simultaneously intruded by igneous bodies. Sill emplacement over the complete extent of a basin would, in reality, span at least hundreds of thousands, if not millions of years [*Jourdan*

Accepted Article

et al., 2008; *Svensen et al.*, 2012] and would result in a decreased estimate of the negative $\delta^{13}C$ excursion over time scales less than a few thousand years.

In summary, our results show that although the amount of thermogenic methane generated in the contact aureole around cooling sills in a sedimentary basin is large enough to influence global climate, the rate at which it is released may be too slow under typical circumstances to account for negative $\delta^{13}C$ excursion over short time scales as observed in the fossil record (<10000 years). The degassing rates can be dramatically increased only if a few crucial factors are taken into consideration and occur simultaneously. Fast degassing rates may be obtained if the permeability structure in the basin is relatively high and cooling of the intruded sill generates fractures which facilitate the complete release of methane trapped below the sill. Additionally, the emplacement of shallow sills may increase the likelihood of explosive venting at the surface as fluids boil during upward migration. Lastly, and most importantly, sill emplacement on the basin-scale would have to occur over relatively short time scales in order to generate the huge amounts of methane required to trigger the observed $\delta^{13}C$ excursion. It is, therefore, likely that the characteristic climate forcing timescale for such events is controlled by sill emplacement over large regions which occurs on time scales that are an order of magnitude greater than that of methane degassing.

6. Conclusions

We have used a 2D FEM/FVM flow model to evaluate the effect of fluid flow in sedimentary basins with sill intrusions on the structure of hydrothermal vents and the maturation of organic matter in the surrounding host rock including its potential impact on past climate change. Although 3D multiphase models with an accurate EOS describing the CH_4-H_2O system will help to further constrain these results, this first study provides useful insights into the nature of such systems. The model predicts that the location of hydrothermal vents depends solely on the flow pattern without the need for explosive degassing and/or boiling effects and is consistent with geological observations. The merging of fluid flow from the bottom and top edges of the sill result in hydrothermal plumes that are positioned at the lateral edges of the sill. We find that the presence of fluids in the system does not significantly alter potential methane estimates from previous studies but provides important information on the rates at which methane generated at depth may be released into the atmosphere. The study shows that a considerable portion of CH_4 may be trapped below the sill if it is horizontal and impermeable. Additionally, the outgassing of methane at the surface can be divided into three

Accepted Article

distinct stages and can take hundreds of thousands of years. The degassing rates show that although the output of thermogenic methane from the surface into the atmosphere or ocean is significant, the recorded changes in $\delta^{13}C$ values at major past climate events occurring over short periods of time (<10,000 years) cannot be satisfactorily explained by this process alone. It is, therefore, likely that methane from organic cracking in sediments during sill intrusion in conjunction with other processes such as volcanic degassing and the destabilization of methane hydrates is responsible for such short term climate change.

Acknowledgements

The authors would like to thank John Higgins and Henrik Svensen for their constructive reviews and comments. KI would also like to thank Jörg Hasenclever for the helpful discussions on modeling aspects presented in this manuscript.

Accepted Article

References

Aarnes, I., H. Svensen, J. A. D. Connolly, and Y. Y. Podladchikov (2010), How contact metamorphism can trigger global climate changes: Modeling gas generation around igneous sills in sedimentary basins, *Geochimica Et Cosmochimica Acta*, *74*(24), 7179-7195, doi:10.1016/j.gca.2010.09.011.

Axelrod, D. I. (1981), Role of volcanism in climate and evolution, *Geological Society of America Special Papers*, *185*, 1-60, doi:10.1130/SPE185-p1.

Barker, D. S. (2000), Emplacement of a xenolith-rich sill, Lajitas, Texas, *Journal of Volcanology and Geothermal Research*, *104*(1-4), 153-168, doi:10.1016/s0377-0273(00)00204-3.

Beardsmore, G. R., and J. P. Cull (2001), *Crustal heat flow: A guide to measurement and modelling*, 324 pp., Cambridge University Press, Cambridge, UK.

Caddick, M. J., and A. B. Thompson (2008), Quantifying the tectono-metamorphic evolution of pelitic rocks from a wide range of tectonic settings: mineral compositions in equilibrium, *Contributions to Mineralogy and Petrology*, *156*(2), 177-195, doi:10.1007/s00410-008-0280-6.

Chevallier, L., and A. Woodford (1999), Morpho-tectonics and mechanism of emplacement of the dolerite rings and sills of the western Karoo, South Africa, *S. Afr. J. Geol.*, *102*(1), 43-54,

Cohen, A. S., A. L. Coe, and D. B. Kemp (2007), The Late Palaeocene Early Eocene and Toarcian (Early Jurassic) carbon isotope excursions: a comparison of their time scales, associated environmental changes, causes and consequences, *Journal of the Geological Society*, *164*(6), 1093-1108, doi:10.1144/0016-76492006-123.

Connolly, J. A. D., and K. Petrini (2002), An automated strategy for calculation of phase diagram sections and retrieval of rock properties as a function of physical conditions, *Journal of Metamorphic Geology*, *20*(7), 697-708, doi:10.1046/j.1525-1314.2002.00398.x.

Costa, A. (2006), Permeability-porosity relationship: A reexamination of the Kozeny-Carman equation based on a fractal pore-space geometry assumption, *Geophysical Research Letters*, *33*(2), L02318, doi:10.1029/2005gl025134.

Courtillot, V. E., and P. R. Renne (2003), On the ages of flood basalt events, *Comptes Rendus Geosciences*, *335*(1), 113-140, doi:10.1016/S1631-0713(03)00006-3.

Dickens, G. R., M. M. Castillo, and J. C. G. Walker (1997), A blast of gas in the latest Paleocene: Simulating first-order effects of massive dissociation of oceanic methane hydrate, *Geology*, *25*(3), 259-262, doi:10.1130/0091-7613(1997)025<0259:abogit>2.3.co;2.

Accepted Article

Accepted Article

Dickens, G. R., J. R. O'Neil, D. K. Rea, and R. M. Owen (1995), Dissociation of Oceanic Methane Hydrate as a Cause of the Carbon Isotope Excursion at the End of the Paleocene, *Paleoceanography*, *10*(6), 965-971, doi:10.1029/95pa02087.

Doyen, P. M. (1988), Permeability, conductivity, and pore geometry of sandstone, *Journal of Geophysical Research: Solid Earth*, *93*(B7), 7729-7740, doi:10.1029/JB093iB07p07729.

Ehrenberg, S. N., G. P. Eberli, and G. Baechle (2006), Porosity–permeability relationships in Miocene carbonate platforms and slopes seaward of the Great Barrier Reef, Australia (ODP Leg 194, Marion Plateau), *Sedimentology*, *53*(6), 1289-1318, doi:10.1111/j.1365-3091.2006.00817.x.

Galerne, C. Y., E.-R. Neumann, and S. Planke (2008), Emplacement mechanisms of sill complexes: Information from the geochemical architecture of the Golden Valley Sill Complex, South Africa, *Journal of Volcanology and Geothermal Research*, *177*(2), 425-440, doi:10.1016/j.jvolgeores.2008.06.004.

Galerne, C. Y., O. Galland, E.-R. Neumann, and S. Planke (2011), 3D relationships between sills and their feeders: evidence from the Golden Valley Sill Complex (Karoo Basin) and experimental modelling, *Journal of Volcanology and Geothermal Research*, *202*(3-4), 189-199, doi:10.1016/j.jvolgeores.2011.02.006.

Galland, O., S. Planke, E. R. Neumann, and A. Malthe-Sorenssen (2009), Experimental modelling of shallow magma emplacement: Application to saucer-shaped intrusions, *Earth and Planetary Science Letters*, *277*(3-4), 373-383, doi:10.1016/j.epsl.2008.11.003.

Galushkin, Y. I. (1997), Thermal effects of igneous intrusions on maturity of organic matter: A possible mechanism of intrusion, *Organic Geochemistry*, *26*(11-12), 645-658,

Ganino, C., and N. T. Arndt (2009), Climate changes caused by degassing of sediments during the emplacement of large igneous provinces, *Geology*, *37*(4), 323-326, doi:10.1130/g25325a.1.

Geiger, S., S. Roberts, S. K. Matthäi, C. Zoppou, and A. Burri (2004), Combining finite element and finite volume methods for efficient multiphase flow simulations in highly heterogeneous and structurally complex geologic media, *Geofluids*, *4*(4), 284-299, doi:10.1111/j.1468-8123.2004.00093.x.

Higgins, J. A., and D. P. Schrag (2006), Beyond methane: Towards a theory for the Paleocene-Eocene Thermal Maximum, *Earth and Planetary Science Letters*, *245*(3-4), 523-537, doi:10.1016/j.epsl.2006.03.009.

Iyer, K., L. H. Rüpke, and J. P. Morgan (2010), Feedbacks between mantle hydration and hydrothermal convection at ocean spreading centers, *Earth and Planetary Science Letters*, *296*(1-2), 34-44, doi:10.1016/j.epsl.2010.04.037.

Iyer, K., L. H. Rüpke, J. Phipps Morgan, and I. Grevemeyer (2012), Controls of faulting and reaction kinetics on serpentinization and double Benioff zones, *Geochem. Geophys. Geosyst.*, *13*, Q09010, doi:10.1029/2012gc004304.

Jamtveit, B., H. Svensen, Y. Y. Podladchikov, and S. Planke (2004), Hydrothermal vent complexes associated with sill intrusions in sedimentary basins, in *Physical Geology of High-Level Magmatic Systems*, edited by C. Breitkreuz and N. Petford, pp. 233-241, Geological Soc Publishing House, Bath.

Jourdan, F., G. Féraud, H. Bertrand, M. K. Watkeys, and P. R. Renne (2008), The 40Ar/39Ar ages of the sill complex of the Karoo large igneous province: Implications for the Pliensbachian-Toarcian climate change, *Geochemistry, Geophysics, Geosystems*, *9*(6), Q06009, doi:10.1029/2008gc001994.

Kurtz, A. C., L. R. Kump, M. A. Arthur, J. C. Zachos, and A. Paytan (2003), Early Cenozoic decoupling of the global carbon and sulfur cycles, *Paleoceanography*, *18*(4), doi:10.1029/2003pa000908.

Küspert, W. (1982), Environmental Changes During Oil Shale Deposition as Deduced from Stable Isotope Ratios, in *Cyclic and Event Stratification*, edited by G. Einsele and A. Seilacher, pp. 482-501, Springer Berlin Heidelberg.

Malthe-Sorenssen, A., S. Planke, H. Svensen, and B. Jamtveit (2004), Formation of saucer-shaped sills, in *Physical Geology of High-Level Magmatic Systems*, edited by C. Breitkreuz and N. Petford, pp. 215-227, Geological Soc Publishing House, Bath.

Pagani, M., K. Caldeira, D. Archer, and J. C. Zachos (2006), An ancient carbon mystery, *Science*, *314*(5805), 1556-1557, doi:10.1126/science.1136110.

Planke, S., T. Rasmussen, S. S. Rey, and R. Myklebust (2005), Seismic characteristics and distribution of volcanic intrusions and hydrothermal vent complexes in the Vøring and Møre basins in *Petroleum Geology: North-western Europe and global perspectives - Proceedings of the 6th Petroleum Geology Conference.*, edited by A. G. Doré and B. A. Vining, Geological Society, London.

Polteau, S., A. Mazzini, O. Galland, S. Planke, and A. Malthe-Sorenssen (2008), Saucer-shaped intrusions: Occurrences, emplacement and implications, *Earth and Planetary Science Letters*, *266*(1-2), 195-204, doi:10.1016/j.epsl.2007.11.015.

Accepted Article

Reece, J. S., P. B. Flemings, B. Dugan, H. Long, and J. T. Germaine (2012), Permeability-porosity relationships of shallow mudstones in the Ursa Basin, northern deepwater Gulf of Mexico, *Journal of Geophysical Research: Solid Earth*, *117*(B12), B12102, doi:10.1029/2012jb009438.

Retallack, Gregory J., and A. H. Jahren (2008), Methane Release from Igneous Intrusion of Coal during Late Permian Extinction Events, *The Journal of Geology*, *116*(1), 1-20, doi:10.1086/524120.

Revil, A., and L. M. Cathles (1999), Permeability of shaly sands, *Water Resources Research*, *35*(3), 651-662, doi:10.1029/98wr02700.

Setzmann, U., and W. Wagner (1991), A new equation of state and tables of thermodynamic properties for methane covering the range from the melting line to 625K at pressures up to 1000MPa, *Journal of Physical and Chemical Reference Data*, *20*(6), 1061-1155, doi:10.1063/1.555898

Svensen, H., and B. Jamtveit (2010), Metamorphic Fluids and Global Environmental Changes, *ELEMENTS*, *6*(3), 179-182, doi:10.2113/gselements.6.3.179.

Svensen, H., S. Planke, B. Jamtveit, and T. Pedersen (2003), Seep carbonate formation controlled by hydrothermal vent complexes: a case study from the Voring Basin, the Norwegian Sea, *Geo-Marine Letters*, *23*(3-4), 351-358, doi:10.1007/s00367-003-0141-2.

Svensen, H., B. Jamtveit, S. Planke, and L. Chevallier (2006), Structure and evolution of hydrothermal vent complexes in the Karoo Basin, South Africa, *Journal of the Geological Society*, *163*, 671-682, doi:10.1144/1144-764905-037.

Svensen, H., F. Corfu, S. Polteau, O. Hammer, and S. Planke (2012), Rapid magma emplacement in the Karoo Large Igneous Province, *Earth and Planetary Science Letters*, *325*, 1-9, doi:10.1016/j.epsl.2012.01.015.

Svensen, H., S. Planke, L. Chevallier, A. Malthe-Sørenssen, F. Corfu, and B. Jamtveit (2007), Hydrothermal venting of greenhouse gases triggering Early Jurassic global warming, *Earth and Planetary Science Letters*, *256*(3-4), 554-566, doi:10.1016/j.epsl.2007.02.013.

Svensen, H., S. Planke, A. Malthe-Sorenssen, B. Jamtveit, R. Myklebust, T. Rasmussen Eidem, and S. S. Rey (2004), Release of methane from a volcanic basin as a mechanism for initial Eocene global warming, *Nature*, *429*(6991), 542-545, doi:10.1038/nature02566.

Svensen, H., S. Planke, A. G. Polozov, N. Schmidbauer, F. Corfu, Y. Y. Podladchikov, and B. Jamtveit (2009), Siberian gas venting and the end-Permian environmental crisis, *Earth and Planetary Science Letters*, *277*(3-4), 490-500, doi:10.1016/j.epsl.2008.11.015.

Accepted Article

Accepted Article

Sweeney, J., and A. K. Burnham (1990), Evaluation of a simple model of vitrinite reflectance based on chemical kinetics, *AAPG Bulletin*, *74*(10), 1559-1570,

Vogt, P. R. (1972), Evidence for global synchronism in mantle plume convection, and possible significance for geology, *Nature*, *240*(5380), 338-&, doi:10.1038/240338a0.

Wignall, P. B. (2001), Large igneous provinces and mass extinctions, *Earth-Science Reviews*, *53*(1-2), 1-33,

Zhou, M.-F., J. Malpas, X.-Y. Song, P. T. Robinson, M. Sun, A. K. Kennedy, C. M. Lesher, and R. R. Keays (2002), A temporal link between the Emeishan large igneous province (SW China) and the end-Guadalupian mass extinction, *Earth and Planetary Science Letters*, *196*(3-4), 113-122, doi:10.1016/S0012-821X(01)00608-2.

Accepted Article

Table 1. List of symbols and values used in the mathematical model

Symbol	Description	Units	Value
A	Frequency factor	s^{-1}	10^{13}
c_{peff}	Effective rock heat capacity	J kg^{-1} K^{-1}	
c_{pf}	Fluid heat capacity	J kg^{-1} K^{-1}	EOS
c_{pm}	Melt heat capacity	J kg^{-1} K^{-1}	820
c_p	Host rock capacity	J kg^{-1} K^{-1}	850
E	Activation energy	J mol^{-1}	
f	Weighting factor		
g	Gravitational acceleration	m s^{-2}	9.81
L_c	Latent heat of crystallization	KJ kg^{-1}	320
L_D	Latent heat of dehydration	KJ kg^{-1}	2800
L_{OM}	Latent heat of organic cracking	KJ kg^{-1}	375
k	Permeability	m^2	
k_0	Permeability constant	m^2	10^{-12} - 10^{-15}
M_{CH4}	Mass of methane per unit volume	kg m^{-3}	
m_{CH4}	Conversion factor from C to CH_4		1.34
m	constant		10^{-3}
n	constant		1.5
P	Fluid pressure	Pa	
R	Gas constant	J K^{-1} mol^{-1}	8.31
R_D	Rate of water generated by dehydration reactions	kg m^{-3} s^{-1}	
R_{OM}	Rate of cracked organic matter	kg m^{-3} s^{-1}	
R_{CH4}	Rate of methane generated by organic cracking	kg m^{-3} s^{-1}	
T	Temperature	K	
T_L	Liquidus temperature	K	1423
T_S	Solidus temperature	K	1223
t	Time	s	
$\vec{v}_f$	Darcy velocity	m s^{-1}	
W	Fraction of convertible organic matter		0.85
Wa	Water content in sedimentary rock		
α_f	Fluid thermal expansion coefficient	K^{-1}	EOS
β_f	Fluid compressibility	Pa^{-1}	EOS
ϕ	Porosity		
ϕ_s	Surface porosity		0.3
μ_f	Fluid viscosity	Pa s	EOS
ρ_f	Fluid density	kg m^{-3}	EOS
ρ_{hr}	Host rock density	kg m^{-3}	2400

ρ_m	Melt density	kg m^{-3}	2600

Table 2. Methane generation potential in simulations without methane transport with varying parameters

Permeability constant	TOC content (wt%)	Methane generated in domain (tons)	Vøring and Møre basin equivalent (Gt)	Western Karoo basin equivalent (Gt)
Diffusion only	5	130,000	2200	1300
Diffusion only	6	165,000	2700	1600
Diffusion only	10	250,000	4100	2400
10^{-12}	5	200,000	3300	2000
$5x10^{-13}$	5	170,000	2900	1700
$5x10^{-13}$	6	200,000	3300	2000
$5x10^{-13}$	10	310,000	5200	3000
10^{-13}	5	155,000	2500	1500
10^{-13}	6	170,000	2700	1600
10^{-13}	10	250,000	4100	2500
10^{-14}	5	140,000	2300	1400
10^{-15}	5	135,000	2300	1300

Table 3. Surface methane fluxes and associated time scales in simulations with methane transport with varying parameters (TOC content = 5 wt%)

Permeability constant (tilt angle)	Methane generated in domain (tons)	Stage 1 (flux normalized to total generated)	Stage 1 + 2 (flux normalized to total generated)	Stage 1-3; experiment end (flux normalized to total generated)
$5x10^{-13}$ (0°)	180,000	~30% in 0.5 Ky	~75% in 5 Ky	~89% in 100 Ky
$5x10^{-13}$ (0°)*	205,000	~35% in 0.5 Ky	~94% in 4 Ky	100% in 10 Ky
10^{-13} (7.5°)	155,000	~16% in 1.1 Ky	~71% in 25 Ky	~97% in 400 Ky
10^{-13} (0°)	155,000	~20% in 2 Ky	~65% in 40 Ky	~75% in 100 Ky
10^{-13} $(0°)^{+}$	170,000	~14% in 9 Ky	~54% in 80 Ky	~58% in 100 Ky
10^{-13} $(0°)^{++}$	190,000	~10% in 34 Ky	~26% in 100 Ky	-
10^{-13} $(0°)^{+++}$	210,000	~5% in 100 Ky	-	-
10^{-14} (0°)	140,000	~11% in 26 Ky	~54% in 320 Ky	~58% in 400 Ky

*simulation with permeable sill

$^{+}$depth of sill increased by 500m, $^{++}$depth of sill increased by 1000m, $^{++}$depth of sill increased by 1500m

Accepted Article

Accepted Article

Figure Captions

Figure 1. Conceptual sketch of the model domain with boundary conditions. The sketch shows a sill intrusion emplaced instantaneously within a sedimentary basin. Heating of surrounding sediments results in contact metamorphism. Dehydration reaction and organic cracking within the contact aureole releases water and methane which may ultimately reach at the surface through hydrothermal vents.

Fig. 2a is a temperature plot with contours of the domain after 5000 years for the reference case (diffusion only). The contact aureole (%Ro≥1) is described by the magenta contour. Fig. 2b plots the vitrinite reflectance and the methane generated within the gas zone after 5000 years.

Fig. 3a and b plot the temperature and vitrinite reflectance of the domain after 130 years (see section 4.2). Fluids are present in this system and are heated around the sill intrusion. The enlarged inset figure illustrates the fluid flow around the sill (black vectors). Hot fluids from the bottom part of sill flow upwards along the outer sill and meet fluids from the upper part at the edge of the outer sill giving rise to hydrothermal plumes at each outer sill.

Fig. 4a and b plots the temperature and vitrinite reflectance within the domain after 5000 years of fluid flow (see section 4.2). The hydrothermal plumes formed at the outer sill (Fig. 3) reach the surface and vent at low temperatures. Enhanced maturation of organic matter around the outer sill occurs due to the hot, ascending fluids.

Fig. 5 shows the thermal evolution, together with vitrinite reflectance, of the system with high permeabilities (see section 4.2.1). Hydrothermal plumes initially form at the edges of the outer sill as is also observed in systems with lower permeabilities (Figs. 3 and 4). These plumes eventually vent at the surface at higher temperatures (Fig. a). Vigorous convection occurs above the inner sill due to the high permeability structure and these fluids eventually vent at the surface at lower temperatures (Fig. c). The presence of convection cells perturbs the thermal structure and results in a very uneven thermal maturation halo around the emplaced sill.

Fig. 6 plots the rate of methane release and cumulative sum of methane released normalized to the total amount of methane generated for simulations with a permeability constant (k_0) of

10^{-13} m^2. Varying the linear density function of methane-bearing fluids (1, 10 and 50% of pure water) does not significantly affect the rate of methane release at the domain surface.

Figs. 7a and b plot the thermal structure together with the vitrinite reflectance of the system with fluid flow (see section 4.3). The difference is that methane released into the fluids by thermal cracking lowers the fluid density and is transported with the fluid. Due to fluid flow around the sill edges, hot, buoyant, methane-rich fluid collects above the outer sill which then rapidly makes its way to the surface as a hydrothermal plume (Fig. 7c).

Fig. 8a plots the transported methane together with the temperature contours in the system after 646 years. The hydrothermal plumes at the outer sills act as pathways through which methane initially escapes into the atmosphere (Stage 1 in section 5.2). The buoyant, methane-rich fluids above the inner sill form finger-like plumes that grow and coalesce to eventually vent at the surface (Stage 2 in section 5.2). Fig. 8b shows the cooled system after 100,000 years. Most of the methane generated above the sill has already left the system. Very slow seepage of the remaining methane occurs over long periods time (Stage 3 in section 5.3).

Fig. 9 plots the rate of methane release and cumulative sum of methane released normalized to the total amount of methane generated for simulations with varying permeability constants (k_0) and sill tilt. See section 5.3 for details.

Fig. 10a-c plots the rate of methane release and cumulative sum of methane released normalized to the total amount of methane generated for simulations with varying sill emplacement depth. Fig. 10d shows that both, the total amount of methane generated (blue dots) and the rate of methane degassing (red dots), are linearly related to the sill emplacement depth.

Accepted Article

H_2O, CH_4, CO_2, SO_2 outgassing

Pressure = 22 MPa

Sediments (Sandstone, clay, shale, evaporite, carbonate)

Vent complex

Contact metamorphism

Fluid flow and degassing

Sill Intrusion (T = 1150°C)

Outer Sill

Inclined Sheet

Inner Sill

No flow and insulated

No flow and insulated

Constant T; no flow

A

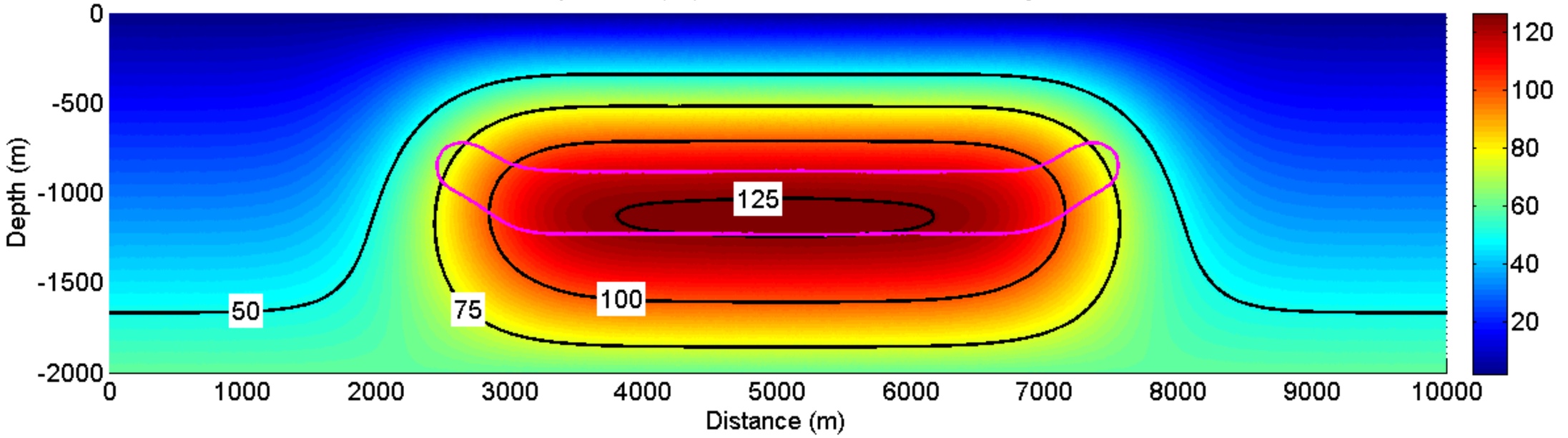
Temperature (°C) with contours at time = 5000 yr
Depth (m)
0
-500
-1000
-1500
-2000
0
1000
2000
3000
4000
5000
6000
7000
8000
9000
10000
Distance (m)
50
75
100
125
120
100
80
60
40
20

B

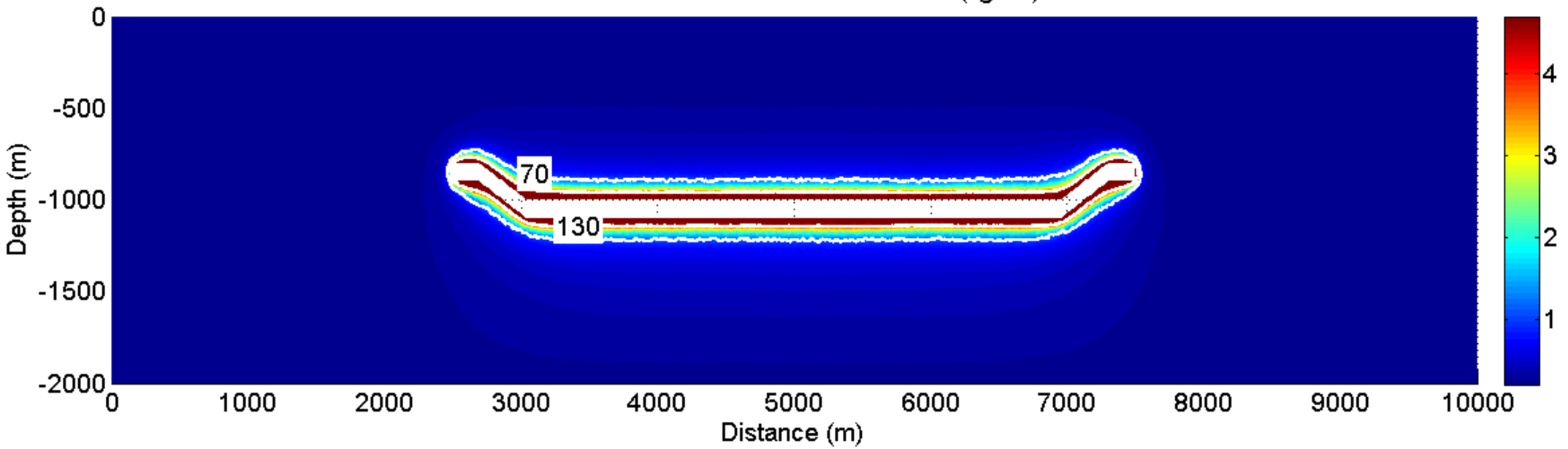
%Ro with methane release contours (kg/m3)
Depth (m)
0
-500
-1000
-1500
-2000
0
1000
2000
3000
4000
5000
6000
7000
8000
9000
10000
Distance (m)
70
130
4
3
2
1

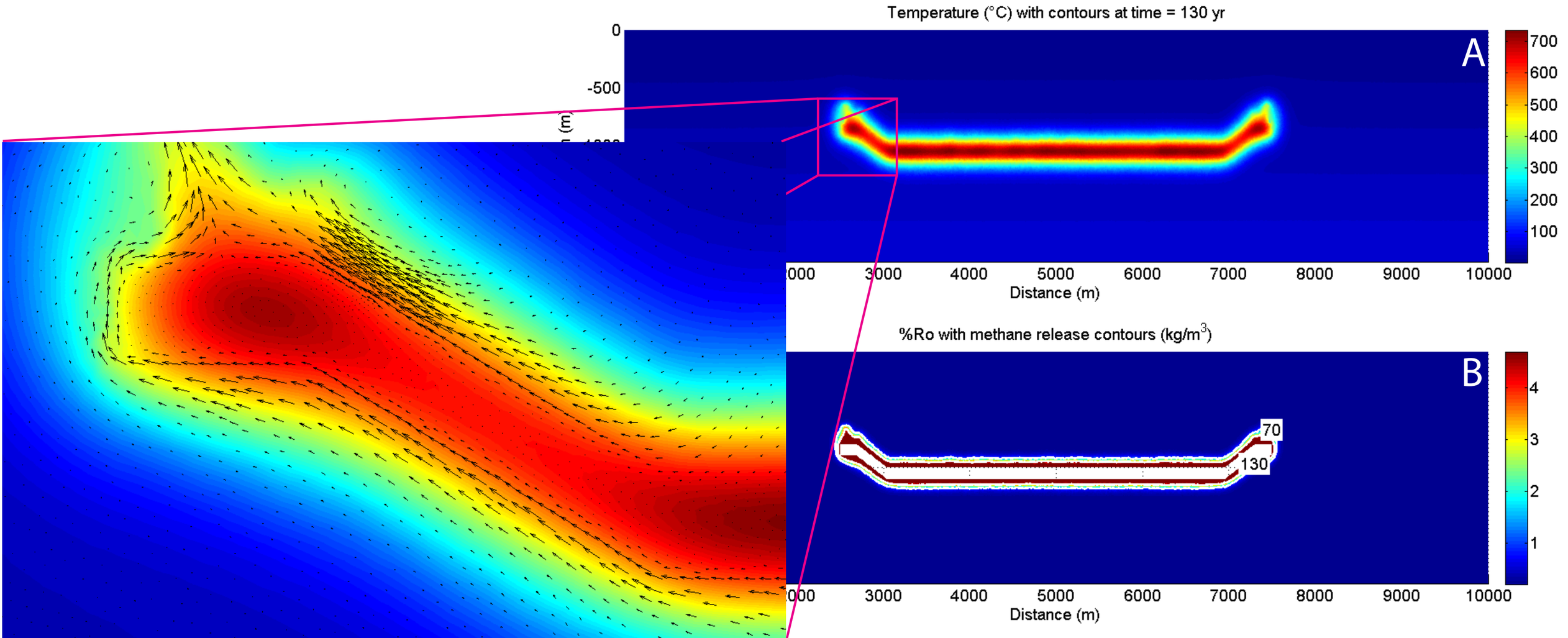
Temperature (°C) with contours at time = 130 yr
A
0
-500
(m)
700
600
500
400
300
200
100
000
3000
4000
5000
6000
7000
8000
9000
10000
Distance (m)
%Ro with methane release contours (kg/m3)
B
70
130
4
3
2
1
000
3000
4000
5000
6000
7000
8000
9000
10000
Distance (m)

A

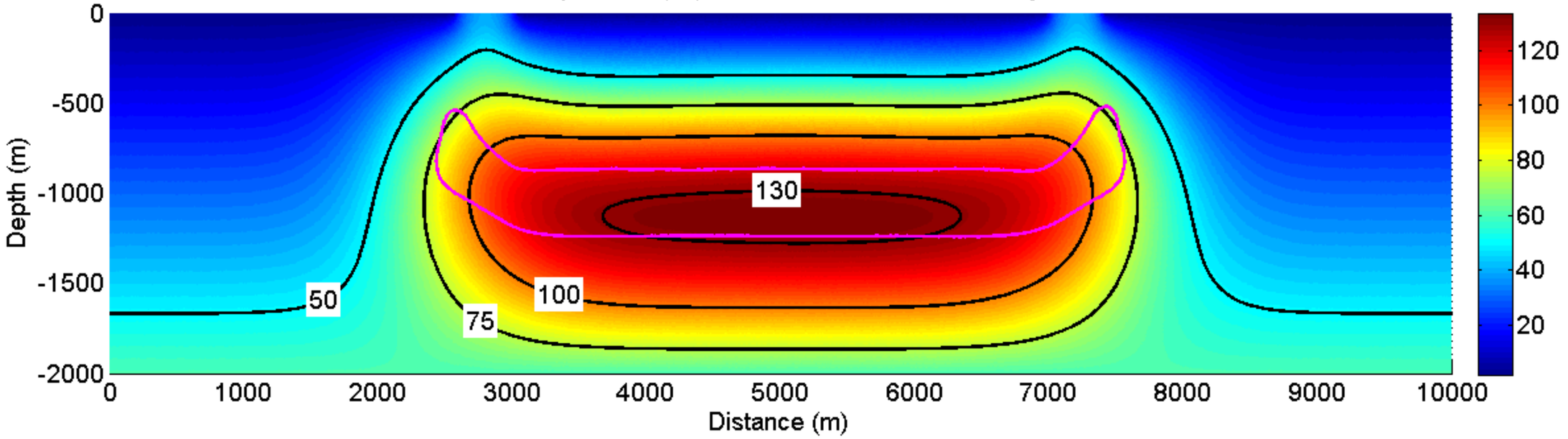
Temperature (°C) with contours at time = 5000 yr
Depth (m)
0
-500
-1000
-1500
-2000
0
1000
2000
3000
4000
5000
6000
7000
8000
9000
10000
Distance (m)
50
75
100
130
120
100
80
60
40
20

B

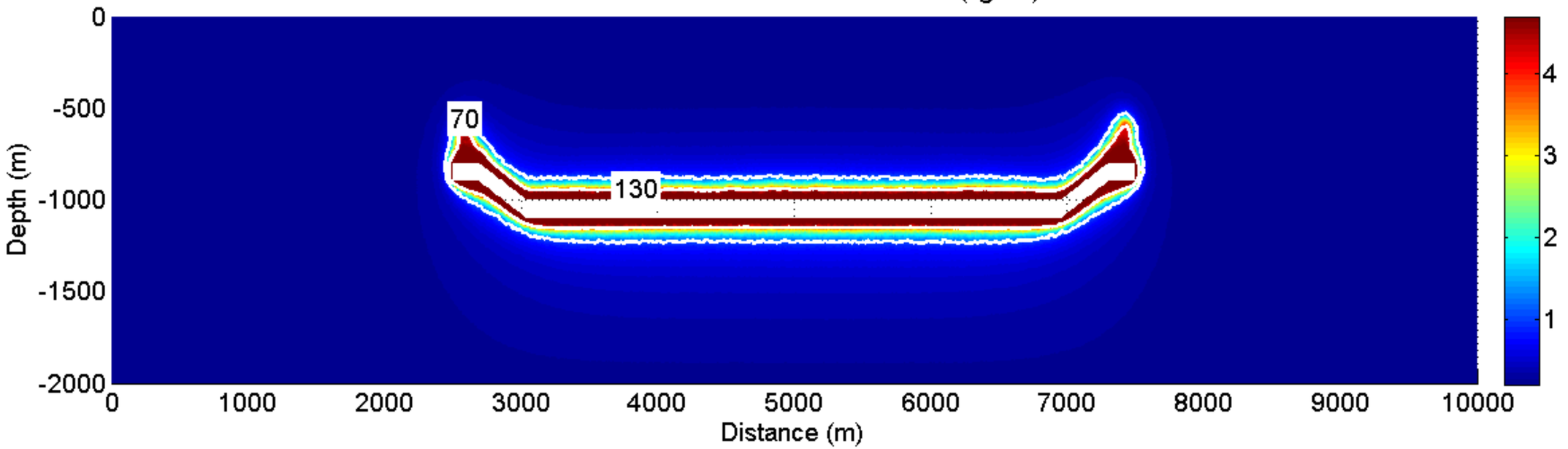
%Ro with methane release contours (kg/m3)
Depth (m)
0
-500
-1000
-1500
-2000
0
1000
2000
3000
4000
5000
6000
7000
8000
9000
10000
Distance (m)
70
130
4
3
2
1

Temperature (°C) with contours at time = 261 yr

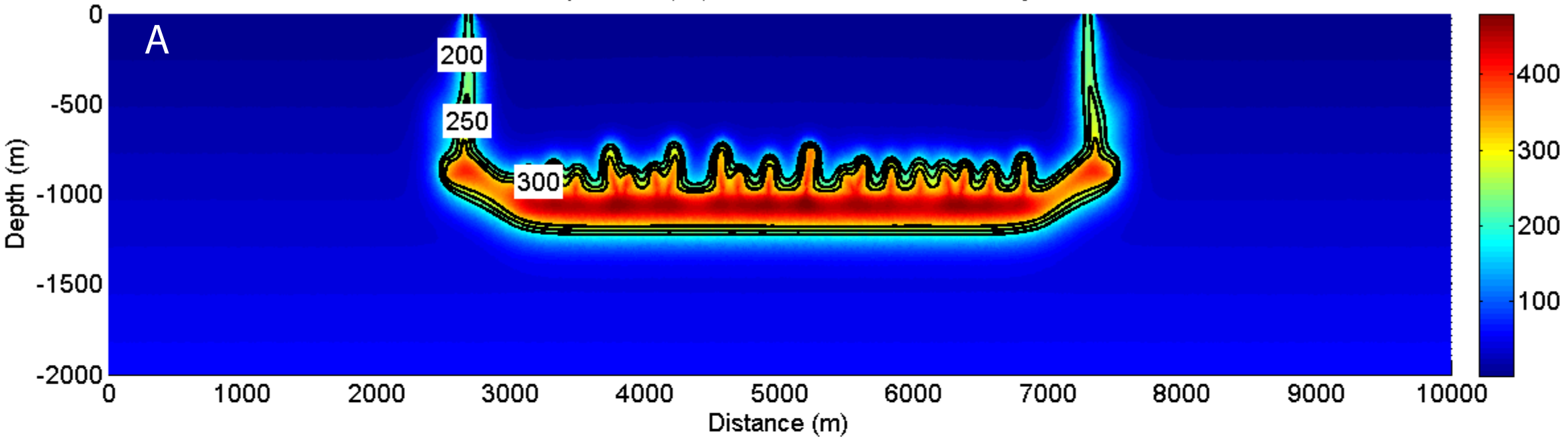

%Ro with methane release contours (kg/m^3)

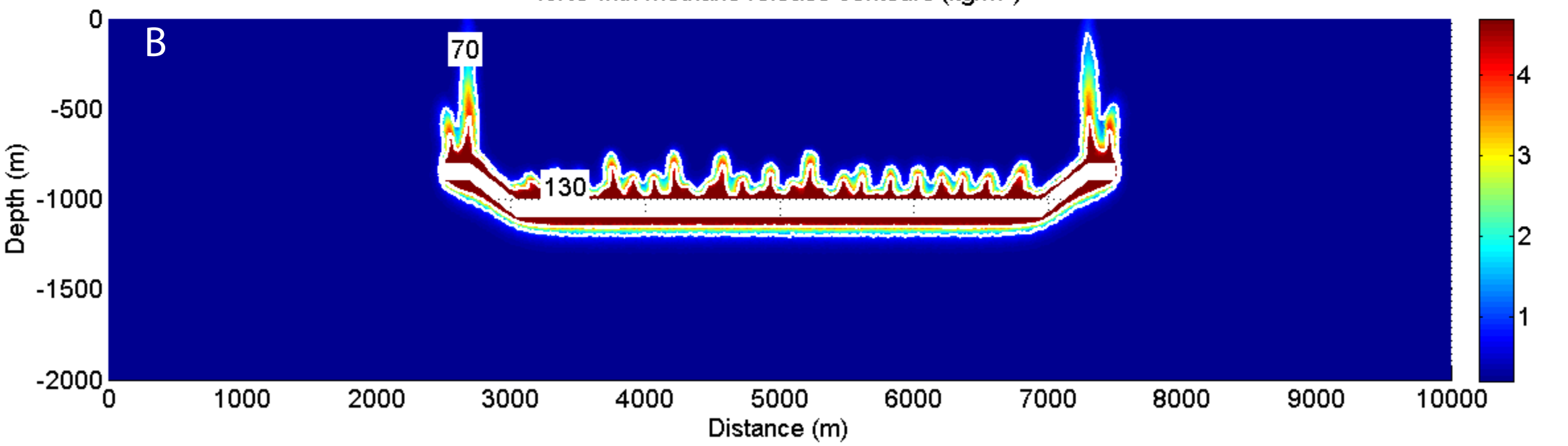

Temperature (°C) with contours at time = 3567 yr

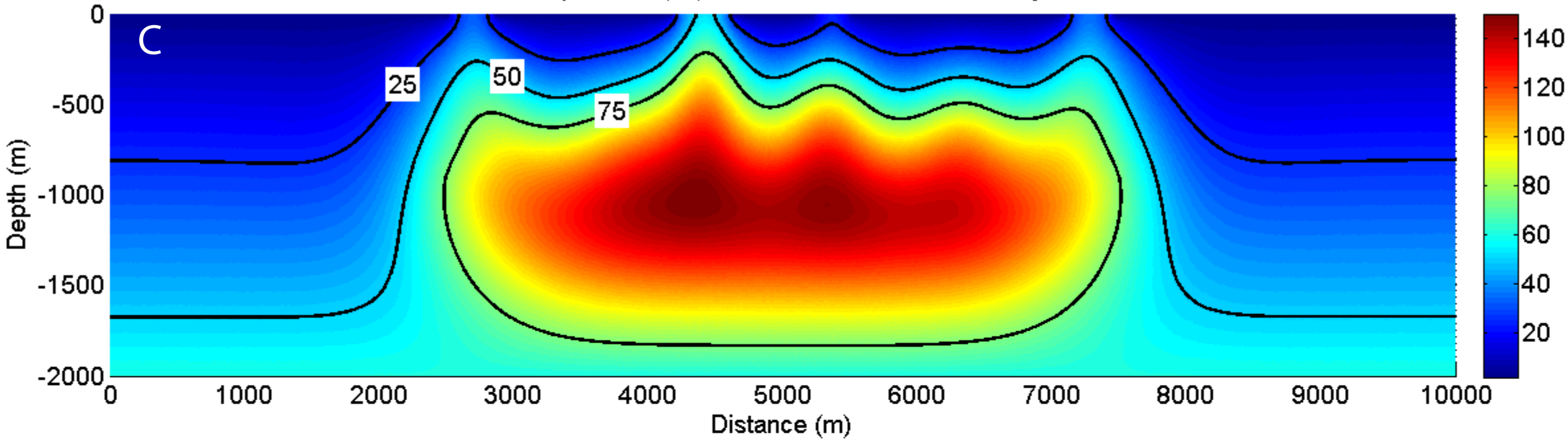

%Ro with methane release contours (kg/m^3)

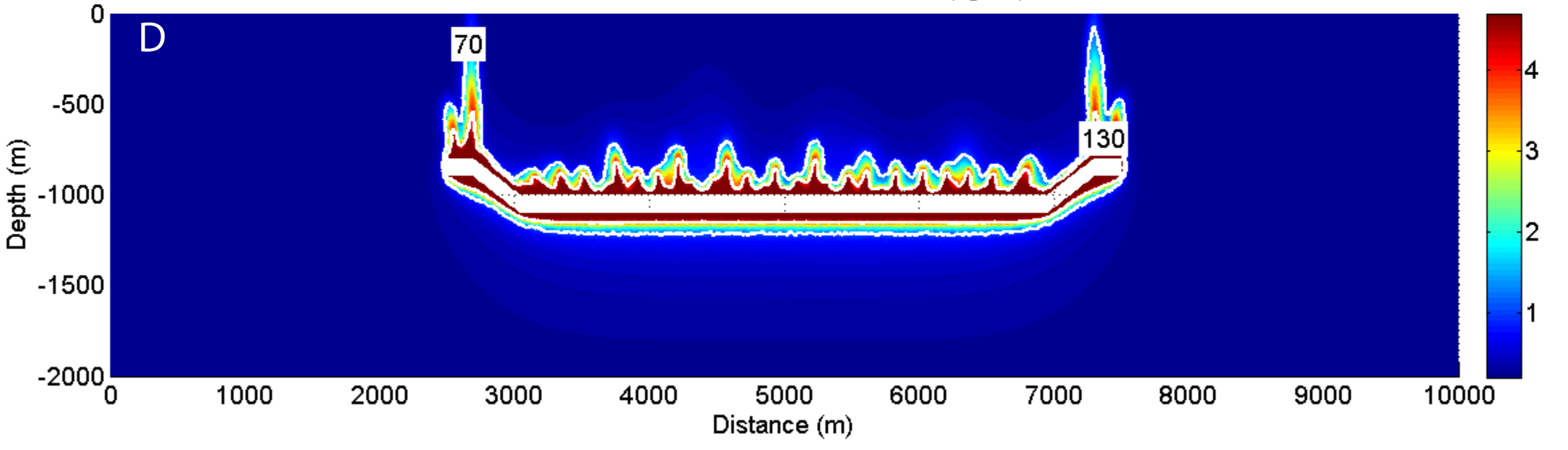

A

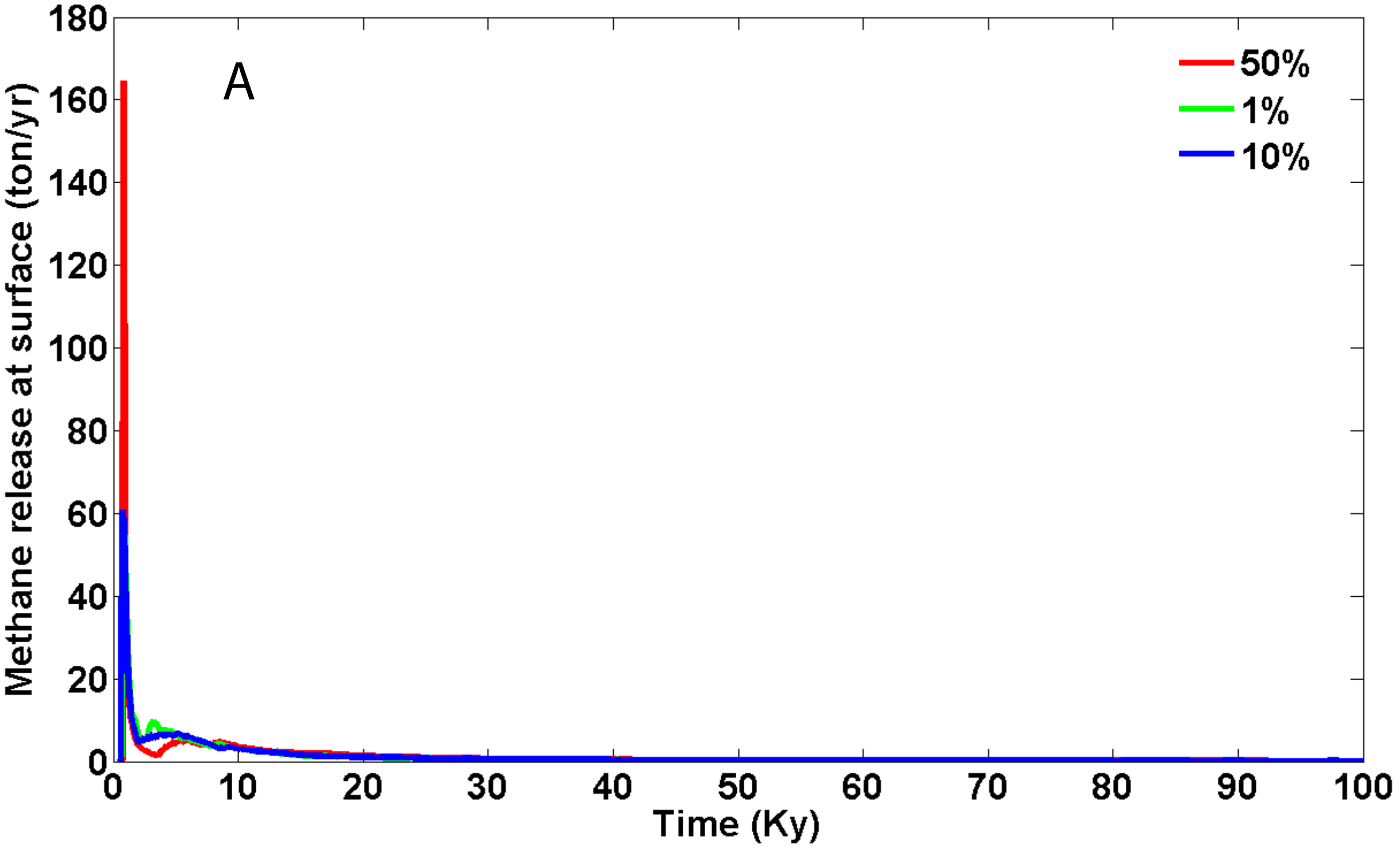
Methane release at surface (ton/yr)
0
20
40
60
80
100
120
140
160
180
0
10
20
30
40
50
60
70
80
90
100
Time (Ky)
50%
1%
10%

B

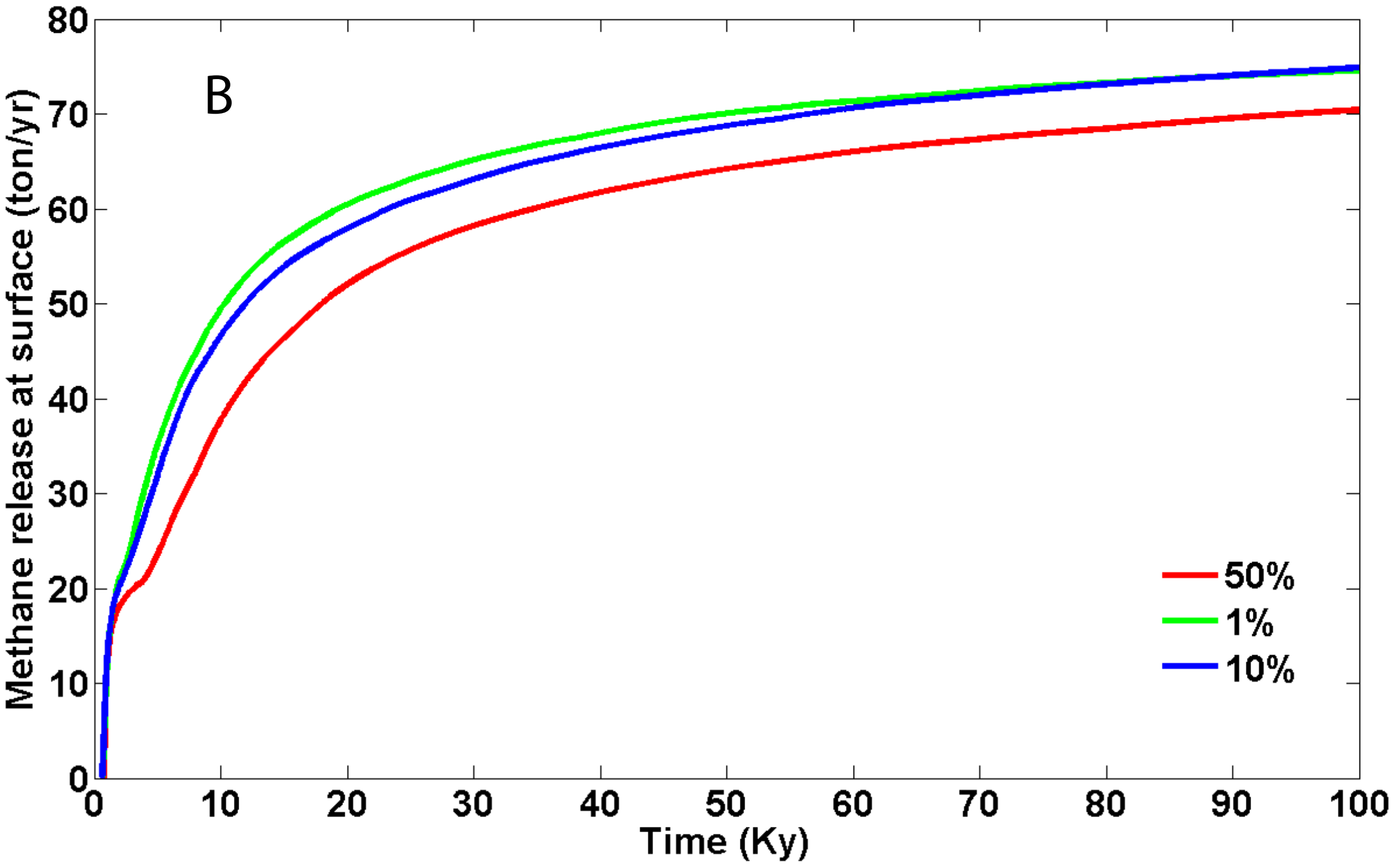
Methane release at surface (ton/yr)
0
10
20
30
40
50
60
70
80
0
10
20
30
40
50
60
70
80
90
100
Time (Ky)
50%
1%
10%

A

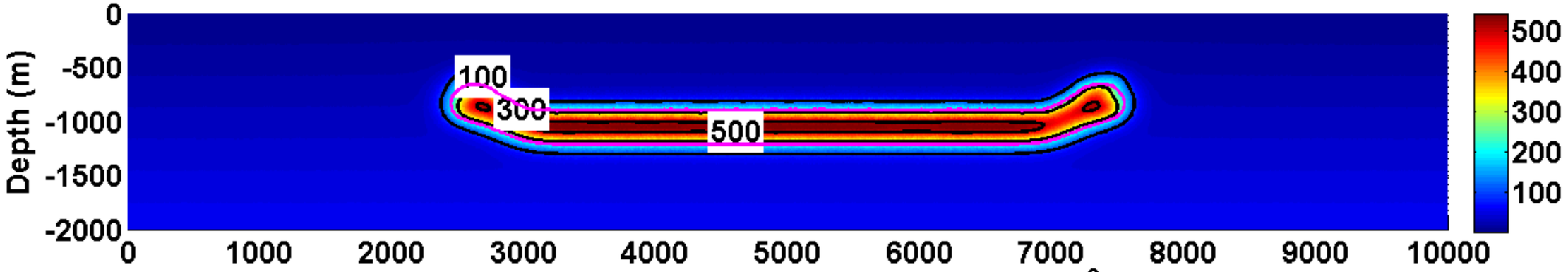
Temperature (°C) with contours at time = 235 yr
Depth (m)
0
-500
-1000
-1500
-2000
100
300
500
0
1000
2000
3000
4000
5000
6000
7000
8000
9000
10000
500
400
300
200
100

B

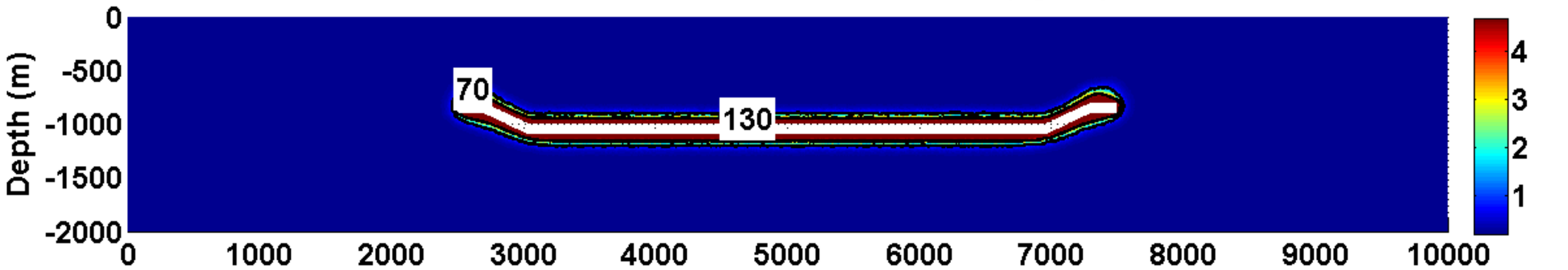
%Ro with methane release contours (kg/m3)
Depth (m)
0
-500
-1000
-1500
-2000
70
130
0
1000
2000
3000
4000
5000
6000
7000
8000
9000
10000
4
3
2
1

C

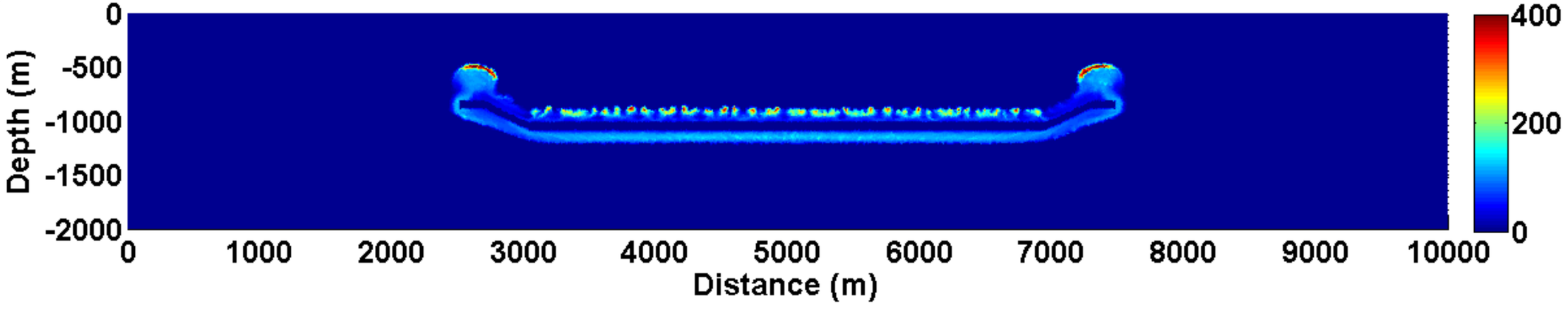
Methane (kg/m3)
Depth (m)
0
-500
-1000
-1500
-2000
0
1000
2000
3000
4000
5000
6000
7000
8000
9000
10000
Distance (m)
400
200
0

A

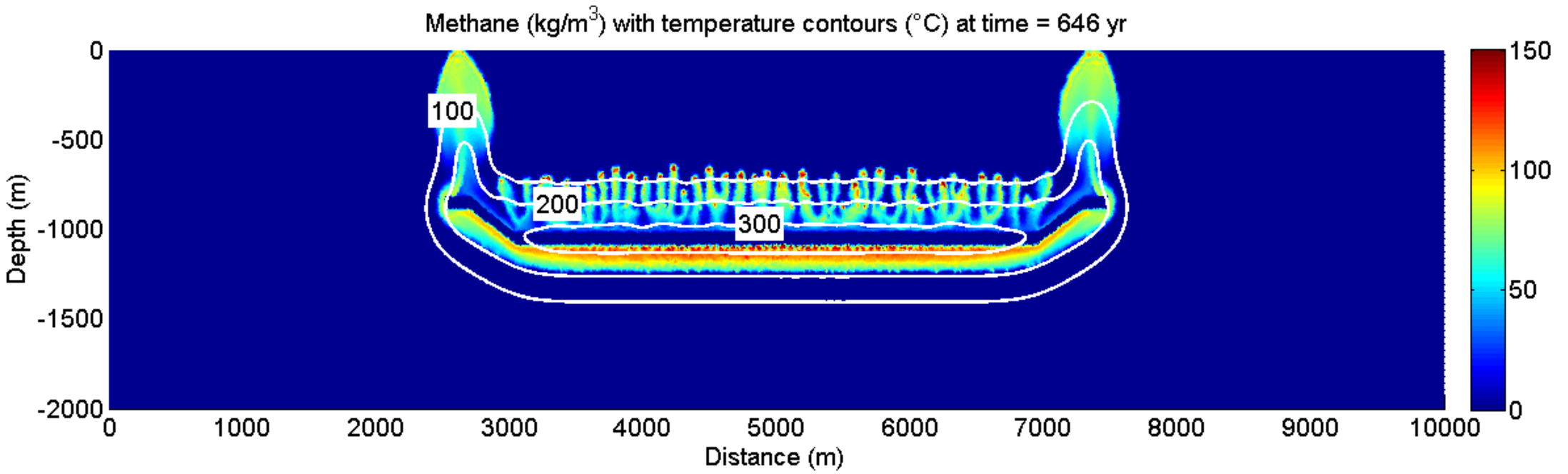
Methane (kg/m3) with temperature contours (°C) at time = 646 yr
100
200
300
Depth (m)
0
-500
-1000
-1500
-2000
0
1000
2000
3000
4000
5000
6000
7000
8000
9000
10000
Distance (m)
150
100
50
0

B

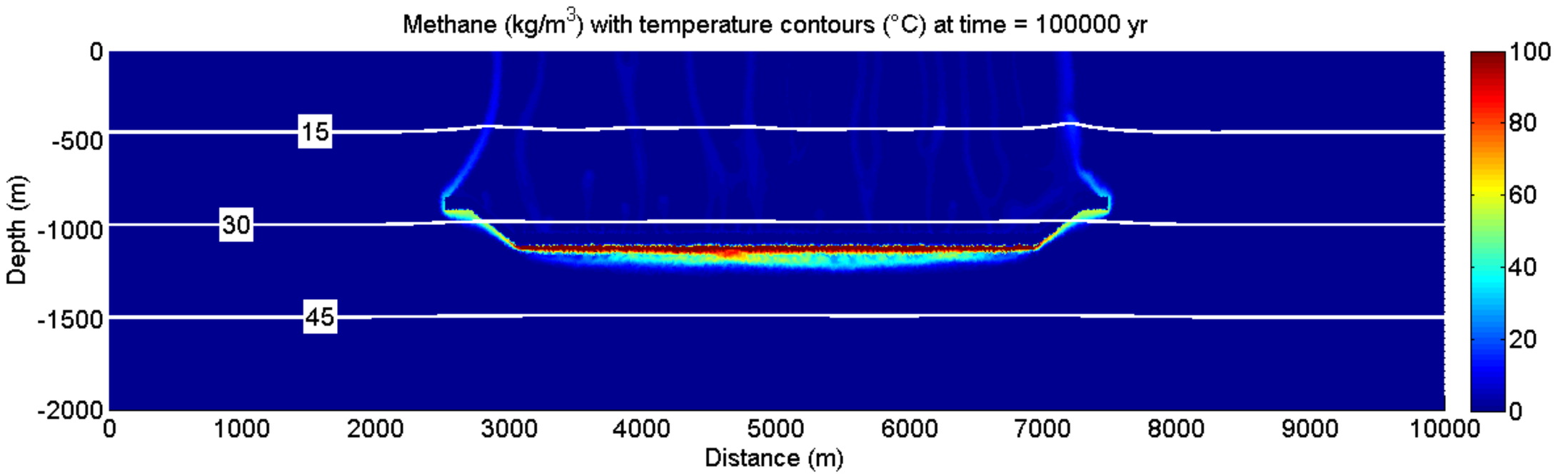
Methane (kg/m3) with temperature contours (°C) at time = 100000 yr
15
30
45
Depth (m)
0
-500
-1000
-1500
-2000
0
1000
2000
3000
4000
5000
6000
7000
8000
9000
10000
Distance (m)
100
80
60
40
20
0

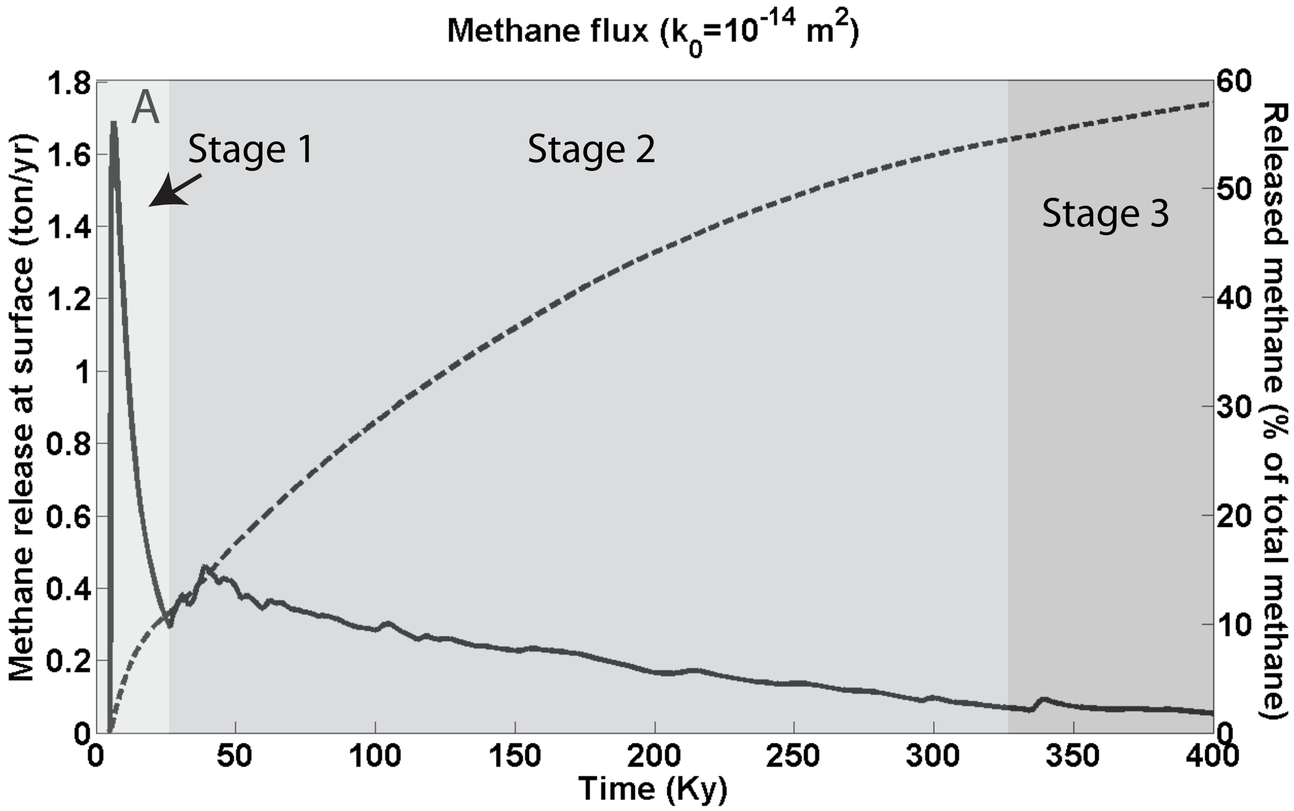
Methane flux (k_0=10^{-14} m^2)
A
Stage 1
Stage 2
Stage 3
Methane release at surface (ton/yr)
Released methane (% of total methane)
Time (Ky)

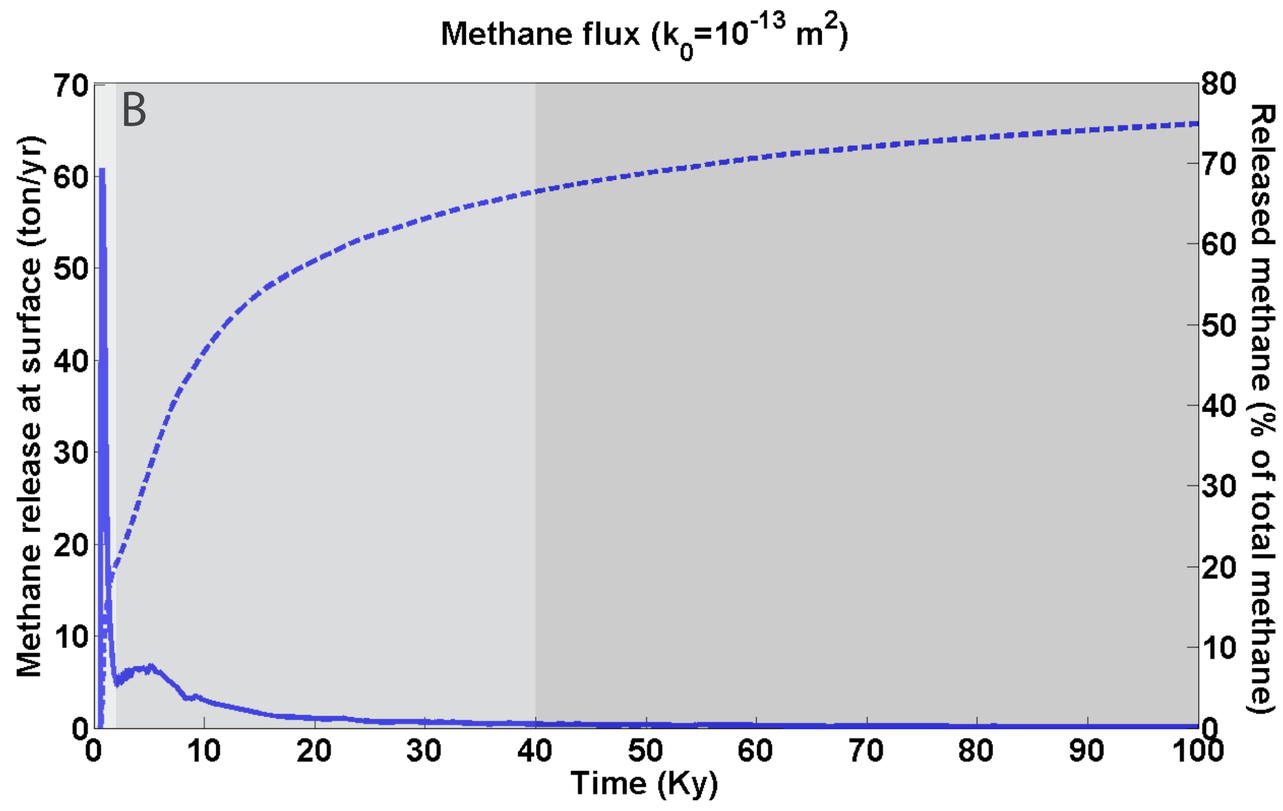
Methane flux (k_0=10^{-13} m^2)
B
Methane release at surface (ton/yr)
Released methane (% of total methane)
Time (Ky)

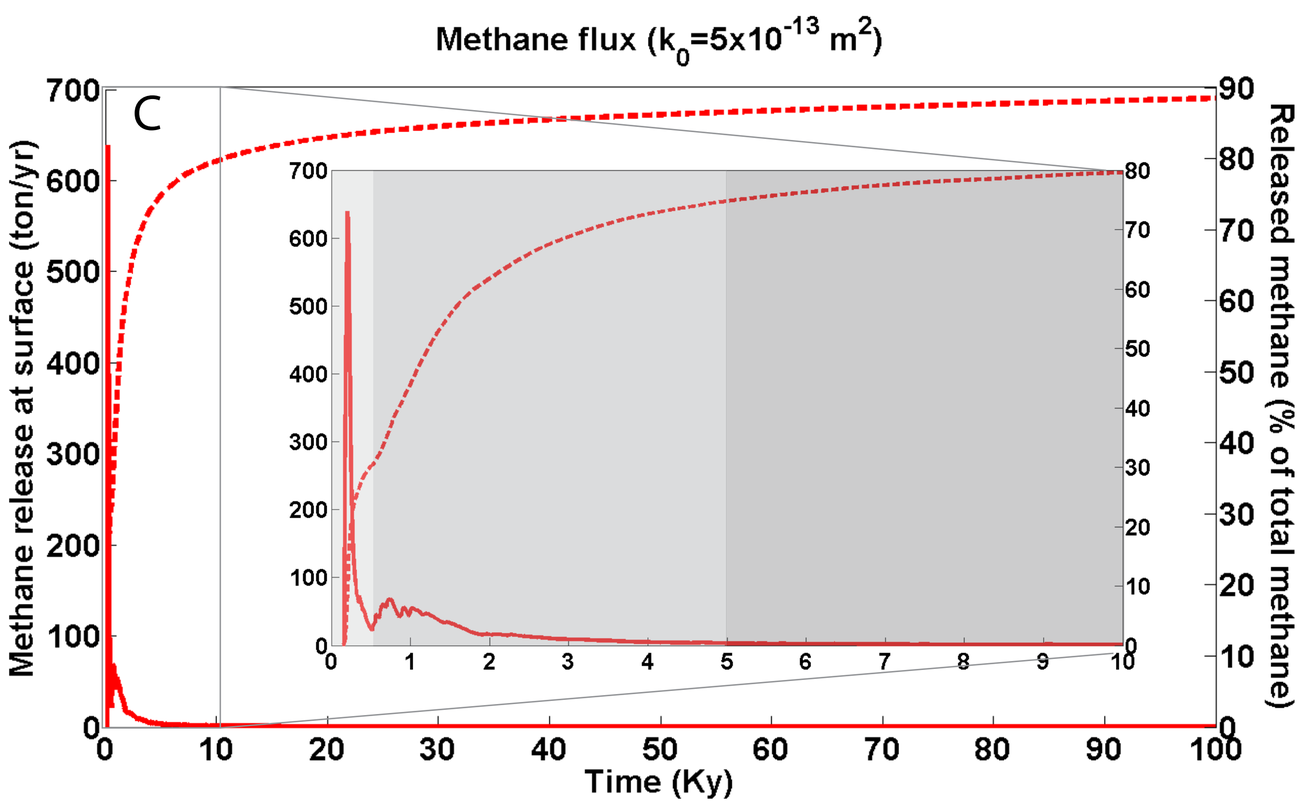
Methane flux (k_0=5x10^{-13} m^2)
C
Methane release at surface (ton/yr)
Released methane (% of total methane)
Time (Ky)

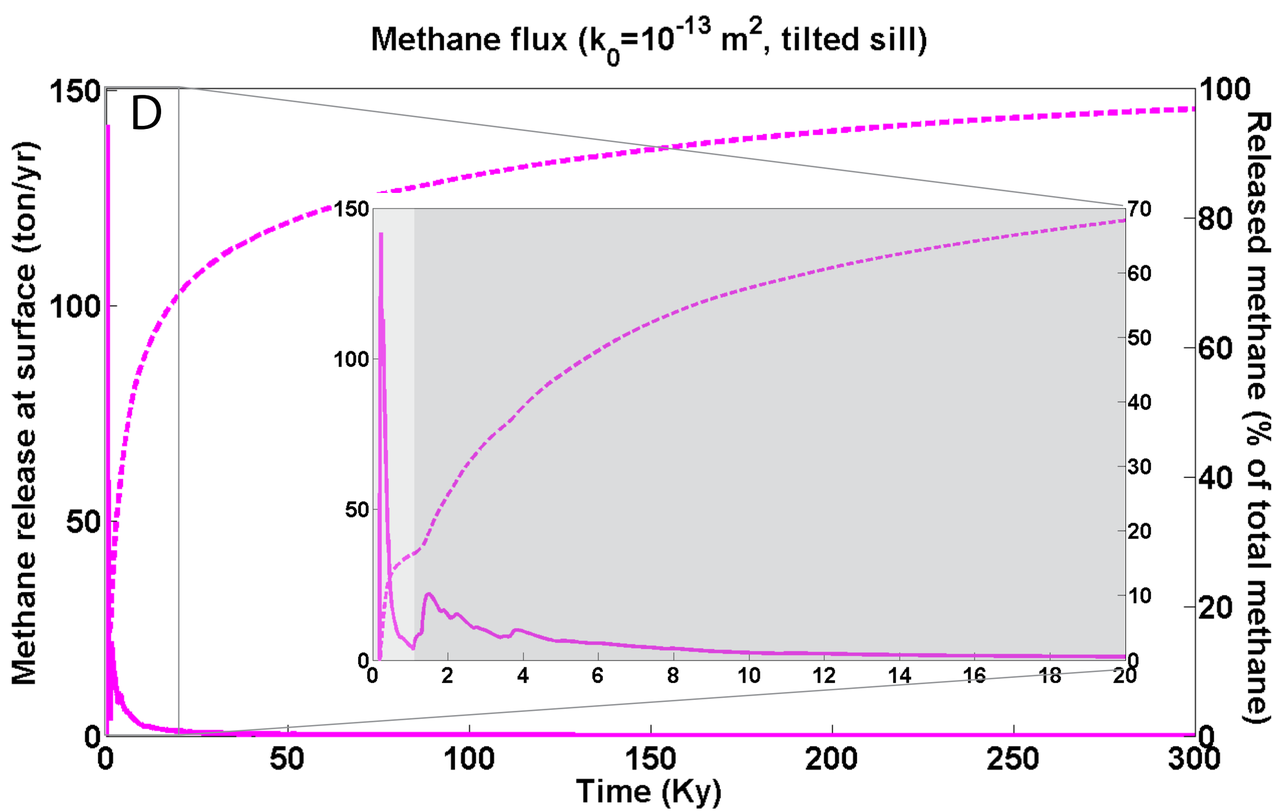
Methane flux (k_0=10^{-13} m^2, tilted sill)
D
Methane release at surface (ton/yr)
Released methane (% of total methane)
Time (Ky)

A

Methane flux (k_0=10^{-13} m^2); sill depth increase = 0.5km

Methane release at surface (ton/yr)

Released methane (% of total methane)

Time (Kyr)

B

Methane flux (k_0=10^{-13} m^2); sill depth increase = 1km

Methane release at surface (ton/yr)

Released methane (% of total methane)

Time (Kyr)

C

Methane flux (k_0=10^{-13} m^2); sill depth increase = 1.5km

Methane release at surface (ton/yr)

Released methane (% of total methane)

Time (Kyr)

D

y(x) = a x + b
a = -0.049
b = 78
R = 0.99447

y(x) = a x + b
a = 0.039136
b = 151.31
R = 0.99426

Total methane generated (Kt)

% of total methane released in 100 Kyr

Increase in sill emplacement depth (m)